MOLECULAR BIOLOGY

XLID syndrome gene Med12 promotes Ig isotype switching through chromatin modification and enhancer RNA regulation

Farazul Haque, Tasuku Honjo*, Nasim A. Begum

The transcriptional coactivator Med12 regulates gene expression through its kinase module. Here, we show a kinase module–independent function of Med12 in CSR. Med12 is essential for super-enhancer activation by collaborating with p300-Jmjd6/Carm1 coactivator complexes. Med12 loss decreases H3K27 acetylation and eRNA transcription with concomitant impairment of AID-induced DNA breaks, S-S synapse formation, and 3′RR-Eμ interaction. CRISPR-dCas9–mediated enhancer activation reestablishes the epigenomic and transcriptional hallmarks of the super-enhancer and fully restores the Med12 depletion defects. Moreover, 3′RR-derived eRNAs are critical for promoting S region epigenetic regulation, synapse formation, and recruitment of Med12 and AID to the IgH locus. We find that XLID syndrome–associated Med12 mutations are defective in both 3′RR eRNA transcription and CSR, suggesting that B and neuronal cells may have cell-specific super-enhancer dysfunctions. We conclude that Med12 is essential for IgH 3′RR activation/eRNA transcription and plays a central role in AID-induced antibody gene diversification and genomic instability in B cells.

INTRODUCTION

Upon antigen encounter, mature B cells undergo immunoglobulin (Ig) class switch recombination (CSR) to allow transition of Ig isotype expression from IgM to IgG, IgA, or IgE (*1*). At the genetic level, the IgM constant gene is replaced by one of the downstream constant genes through Ig locus–specific DNA rearrangement induced by activation-induced deaminase (AID) (*2*, *3*). This programmed DNA arrangement involves three critical steps: (i) GLT through long intronic S regions, (ii) targeted DNA breaks in recombining S regions, and (iii) joining cleaved S region pairs by nonhomologous end joining (NHEJ)–mediated repair (*4*, *5*). AID plays a central role in these processes by inducing DNA cleavage at specific loci and promoting S-S synapse (unique cis conformation) formation to facilitate recombination (*6*, *7*). Although the requirement of AID in DNA cleavage and S-S synapse formation is well established, the precise mechanism of locus specificity and S-S tethering has yet to be fully understood.

The IgH 3′RR super-enhancer region plays an important role in AID-induced CSR (*8*, *9*) and somatic hypermutation (*10*) but not in recombination-activating genes (RAG)-induced V(D)J recombination (*11*). However, how 3′RR cis-regulatory elements influence and/or regulate AID-induced actions during CSR remains poorly understood. The most prevalent and widely accepted view suggests that the 3′RR is mainly involved in GLT (*12*, *13*), which is one of the essential prerequisites that precedes AID-induced CSR. The core 3′RR encompasses four transcriptional enhancers (hs3a, hs1.2, hs3b, and hs4), and deletion of all four decreases the GLTs, with expected decreases in CSR (*9*, *13*). These 3′RR enhancers are thought to function cooperatively, as their individual deletion does not impair Ig isotype switching. However, deletion of both hs3b and hs4 decreases CSR for all isotypes except IgG (*8*). In summary, the precise mechanisms underlying 3′RR-dependent CSR regulation remains unsettled despite studies demonstrating the cumulative activity of individual enhancers, such as hs1.2 and hs4, or in combination with hs3b (*14*).

Enhancers and super-enhancers are typically considered to be distally located gene regulatory elements that enhance transcription by long-distance interaction with gene promoters (*15*, *16*). Enhancer activation requires formation of specific protein complexes that include transcription factors (TFs), co-regulators, chromatin remodelers and modifiers, and RNA polymerase II (RNAPII) (*15*–*17*). One enhancer coactivator is the supramolecular Mediator complex, which serves as a signaling coordinator between transcriptional machinery and RNAPII through modulating subunit composition (*18*, *19*). Mediator is assembled as four subcomplexes referred to as "head," "middle," "tail," and "kinase" modules (*20*, *21*). While the head, middle, and tail modules comprise the core Mediator, the fourth module reversibly interacts with the core through its Med13 subunit. The kinase module is composed of Med12, Med13, Cdk8, and cyclin C and contributes to both negative and positive regulation of RNAPII-driven transcription (*21*–*23*).

The N-terminal leucine-rich (L) domain of Med12 is responsible for cyclin-dependent kinase 8 (CDK8) activation, representing a kinase module–dependent function of Med12 (*24*). Notably, while leukemia- and uterine leiomyoma (UL)–associated mutations are localized within the L domain, X-linked intellectual disability (XLID)–associated mutations, including atypical and typical FG, Lujan, Opitz-Kaveggia, or Ohdo syndrome, are distributed across the central leucine- and serine-rich (LS) domain (*25*). Several prostate cancer–related mutations are also located in the LS as well as proline-, glutamine-, and leucine-rich (PQL) domain (*25*). The PQL domain is adjacent to the LS domain and is subject to arginine methylation at several positions, which likely contributes to noncoding RNA (ncRNA) binding and protein-protein interactions (*26*). In addition, some PQL domain mutations may confer chemotherapeutic resistance in cancer (*27*). Mutations in the C-terminal odd-paired area glutamine-rich (OPA) domain of Med12 has been reported in three siblings with low IgG levels and B cell proliferation

Department of Immunology and Genomic Medicine, Graduate School of Medicine, Kyoto University, Yoshida, Sakyo-Ku, Kyoto 606-8501, Japan.
*Corresponding author. Email: honjo@mfour.med.kyoto-u.ac.jp

defects (*28*). Although Med12 mutations mentioned are thought to be crucial for disease progression, the functional significance and molecular mechanisms of these mutations remain poorly understood.

Here, we use various domain-specific Med12 mutations to determine Med12 structure-function relationships within the context of AID-induced genomic instability in mature B cells. We find that Med12 is dispensable for switch GLT but is indispensable for 3′RR activation and transcription. We also find that these Med12 functions are independent of kinase module function. Mechanistically, Med12, in collaboration with p300 and Jmjd6/coactivator-associated arginine methyltransferase 1 (Carm1) complexes, preserves signature histone epigenetic marks at 3′RR and S regions, resulting in adequate enhancer RNA (eRNA) production and unperturbed CSR. Loss of Med12 leads to both architectural and epigenomic dysregulation of the IgH locus, abrogating AID-induced DNA double-strand breaks (DSBs) and postbreak recombination/repair processes essential for Ig isotype switching.

RESULTS

Med12 is required for AID-induced DNA breaks and S-S synapse formation during CSR

To investigate the requirement of Med12 in CSR, we established a small interfering RNA (siRNA)–mediated Med12 gene knockdown (KD) (Med12^{KD}) model in the murine B cell line CH12F3-2A. This cell line efficiently switches from IgM to IgA in response to stimulation with CD40L, interleukin-4 (IL-4), and transforming growth factor–β (TGF-β) (CIT) (*29*). Multiple siMed12 concentrations effectively inhibited CSR with a clear trend of dose dependency (Fig. 1A and fig S1A). We subsequently used 20 pmol of siMed12 in all the experiments, as it did not affect cell proliferation. To confirm KD specificity, we designed a wild-type Med12 (WT^{R}) construct capable of producing Med12 transcripts resistant to degradation by siMed12 (Fig. 1B, top). Transfection of cells with the Med12 WT^{R} construct showed a dose-dependent CSR complementation in Med12^{KD} cells (Fig. 1B). These results suggest that Med12 plays a critical role in CSR and may be specifically required for effective CSR.

We confirmed that Med12 deficiency did not affect switch GLT, μGLT, and αGLT or AID expression (Fig. 1C and fig. S1A). Consistently, Med12 depletion did not affect AIDER [AID fused with estrogen receptor (ER)] expression but strongly impaired CSR in the AIDER-CH12F3-2A line (fig. S1, B and C). To examine the exact steps of CSR that are impaired following Med12 depletion, we assessed AID-induced DNA DSB formation in the S region by linker ligation-mediated polymerase chain reaction (LM-PCR) (*30*). Med12 depletion results in a sharp decrease in DNA DSB signals, which are restored to control levels with cotransfection of the Med12 WT^{R} construct (Fig. 1D and fig. S1D), suggesting that AID-induced DNA DSB formation requires Med12. Consistently, γH2AX, a marker of early DNA damage response (DDR) signaling, was also diminished at the Sμ and Sα regions in Med12^{KD} cells (Fig. 1E).

IgA CSR requires a unique cis conformation of the IgH locus known as the S-S synapse. This synapse brings the donor Sμ and the acceptor Sα into close proximity by looping out a large intervening sequence region. S-S synapse formation detection assays have included standard chromosome confirmation capture (3C), which enables detection of S-S proximity as a hybrid PCR product of two widely separated loci, namely, Sμ and Sα. Similarly, 3C assays can be used to detect the proximity or long-range interactions between promoters and enhancers (Eμ-3′RR) or interaction with novel loci other than IgH. In Med12^{KD} cells, we find that the intensity of Sμ-Sα hybrid PCR products was strongly decreased (Fig. 1F), suggesting that Med12 is required for proper S-S synapse formation during CSR. Depletion of Med12 also markedly diminished the interaction between Eμ and 3′RR, providing further evidence for the role of Med12 for both constitutive (Eμ-3′RR) and inducible (S-S) locus conformation.

As AID expression induces IgH/c-Myc translocation in addition to CSR in B lymphocytes, we next examined IgH/c-Myc translocation frequency by PCR amplifying translocated genomic DNA junctions from siControl- and siMed12-transfected cells. PCR products were subjected to Southern hybridization using c-Myc locus–specific probe (*31*). Med12 depletion resulted in a reduction of AID-induced IgH/c-Myc translocations (Fig. 1G). Similarly, Med12 depletion also counteracted augmentation of IgH/c-Myc translocations by Topoisomerase 1 (Top1) deficiency.

Ligation of DSB ends between two S regions mainly occurs through the NHEJ-mediated DNA repair pathway; we next examined the impact of Med12 deficiency in an NHEJ-mediated repair assay using *I-Sce*I meganuclease–induced DSBs (*32*). In this assay, a green fluorescent protein (GFP) reporter gene is expressed only after successful NHEJ between two cleaved *I-Sce*I sites, removing an intervening thymidine kinase gene cassette. The *I-Sce*I–expressing plasmid was cotransfected with siControl or siMed12 into the reporter cell line, H1299dA3-1. As expected, in siControl-treated cells, *I-Sce*I expression showed 12.6% GFP CIT (+) cells, which was reduced to 3.4% in siMed12-treated cells, suggesting that DSB end joining via NHEJ requires Med12 (fig. S1E). Together, we conclude that Med12 is vital for promoting AID-induced DNA DSBs, S-S synapse formation, and NHEJ, all of which are essential for Ig isotype switching.

S region DNA break and synapse formation are regulated by distinct domains of Med12

To understand the molecular basis of the diverse functions of Med12, we examined Med12 structure-function relationships by generating several deletion and point mutant constructs. Med12 is a large protein with four distinct domains (Fig. 2A): an L domain, an LS domain, a PQL, and an OPA domain. We generated individual domain-specific deletions using WT^{R} sequence as a template (Fig. 2A). CSR complementation efficiency of these mutants was measured relative to Med12^{KD} cells transfected with the WT^{R} construct. We find that the ΔL^{R}, ΔOPA^{R}, and ΔNLS^{R} (nuclear localization signal) mutants display WT-level CSR complementation, whereas ΔLS^{R} and ΔPQL^{R} show a substantial loss of CSR activity (Fig. 2B). We find that when CSR-defective ΔLS^{R} and ΔPQL^{R} constructs are cotransfected, CSR is restored back to WT^{R} levels (Fig. 2B). However, as individual LS and PQL domains were intact in the respective ΔPQL^{R} and ΔLS^{R} mutants, we suspect that functional cross-complementation occurs between these two domains.

To further examine this possible cross-complementation, we tested whether ΔLS^{R} and ΔPQL^{R} mutants can support AID-induced DNA DSBs and S-S synapse formation by LM-PCR and 3C assays. LM-PCR results suggest that the ΔLS^{R} mutant is severely

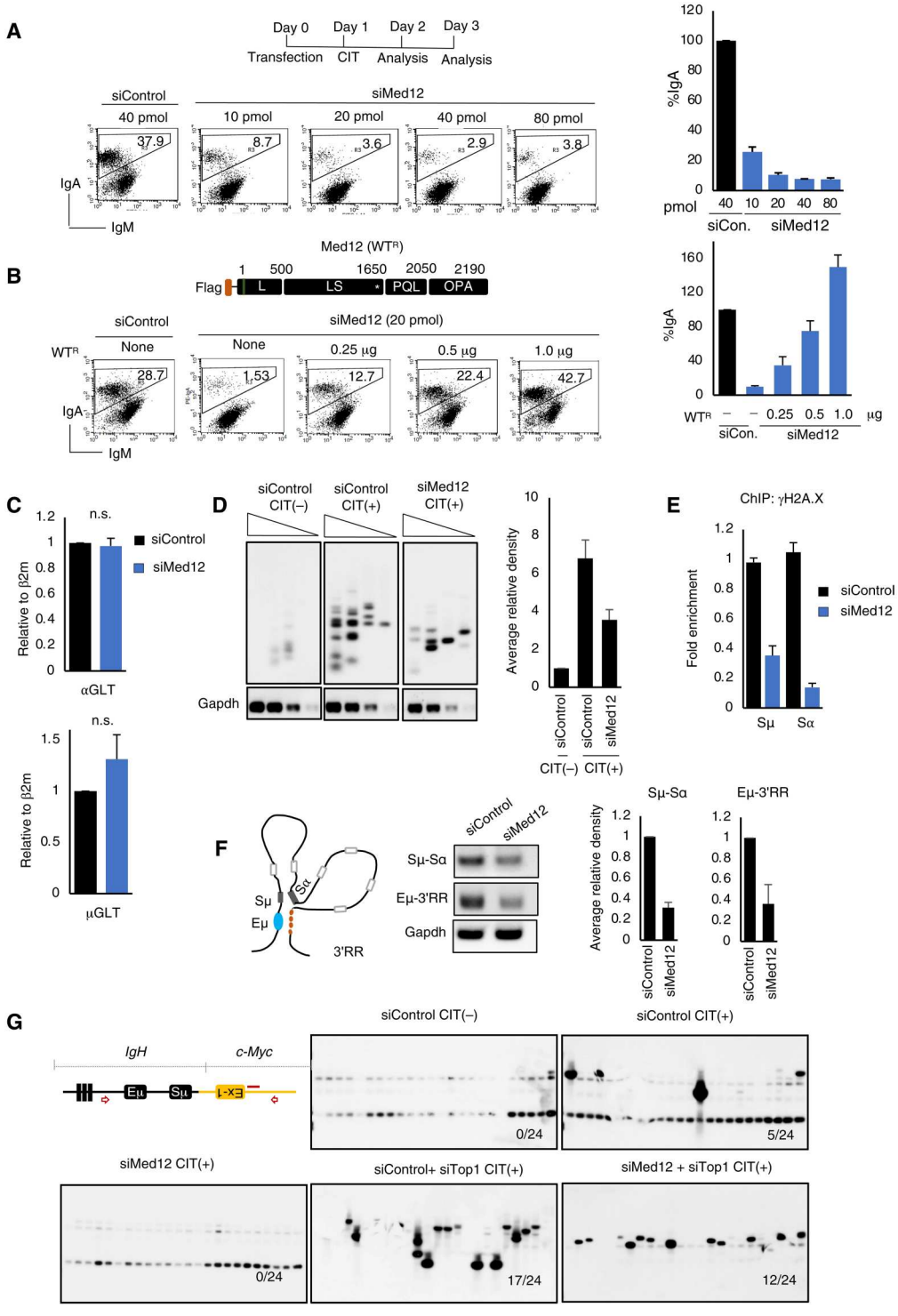

Fig. 1. Med12 depletion leads to impaired AID-induced DNA break, S-S synapse, and IgH/c-Myc translocation. (**A**) The time course of the experiment. CH12F3-2A cells were transfected with either siControl or siMed12 and CIT stimulated CIT (+) as indicated and analyzed by flow cytometry [fluorescence-activated cell sorting (FACS)]. (**B**) Representation of siMed12 resistance wild-type Med12^{R} (WT^{R}) used for the CSR rescue experiment. Asterisk (*) mark shows the site of the si resistance. The FACS analysis showing the effect of different concentrations of WT^{R} on IgA complementation efficiencies. (**C**) The reverse transcription quantitative PCR (RT-qPCR) graph showing the effect of siControl and siMed12 (20 pmol) on germline transcripts after normalization with endogenous β2 microglobulin (β2m). (**D**) LM-PCR showing the amplified Sμ region in respective samples followed by Southern blot analysis with 5′-Sμ–specific probe. Glyceraldehyde-3-phosphate dehydrogenase (GAPDH) of respected samples served as an internal control. The triangles indicate 3× dilution in the DNA amount. Right: The ImageJ analysis showing the normalized band intensities in the respective samples. (**E**) The chromatin immunoprecipitation (ChIP)–qPCR estimating the γH2AX occupancy in Control/siMed12-treated cells. Values were normalized to the DNA input signals followed by the maximum value in each dataset. (**F**) Schematic view of the long-range interactions (LRI) that occurred at the IgH locus after CIT stimulation, which brings Sμ-Sα into close proximity. The representative gel picture of 3C-PCR, detecting the LRI between different IgH regions. GAPDH served as a loading control. Right: The ImageJ analysis showing the normalized band intensities in the respective samples. (**G**) PCR amplification scheme to detect IgH/c-Myc chromosomal translocations. Southern blot analysis of PCR-amplified fragments with a Myc-specific probe in indicated samples. The result summarizes the means ± SD of three independents experiments, and the statistical significance was determined by two-tailed Student's *t* test ($P > 0.05$); n.s. indicates insignificant difference.

defective in S region DSB formation in Med12^{KD} cells, which is consistent with this mutant's CSR deficiency (Fig. 2B). Conversely, S region DNA break signals were detected in Med12^{KD} cells transfected with ΔL^{R}, ΔPQL^{R}, ΔLS^{R} + ΔPQL^{R}, and ΔOPA^{R} mutants (Fig. 2C). Notably, ΔPQL^{R} rescued the severe DNA break defect in ΔLS^{R}-transfected Med12^{KD} cells. Together, we conclude that the LS domain of Med12 plays a critical role in AID-induced S region DNA break.

We next examined the contribution of the ΔLS^{R} and ΔPQL^{R} mutants and their coexpression (ΔLS^{R} + ΔPQL^{R}) in S-S synapse formation. We find that Med12 depletion significantly reduces Sμ-Sα and Eμ-Sα interactions, while WT^{R} transfection of Med12^{KD} cells restores these interactions (Fig. 2D). We find that neither ΔLS^{R}

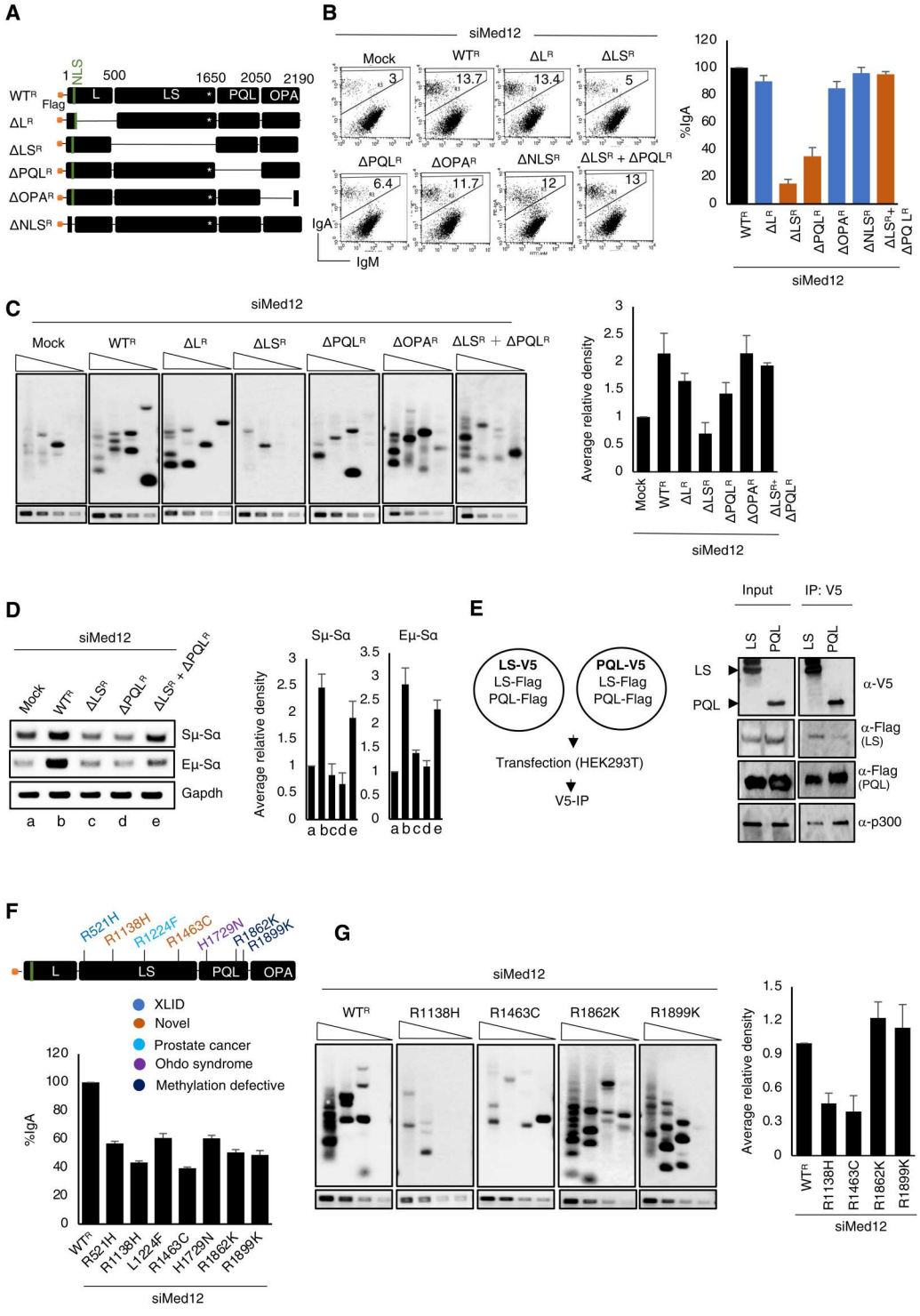

Fig. 2. Med12 regulates CSR differentially by its LS and PQL domains. (**A**) Schematic representation of various Med12 deletion mutants used in the study. (**B**) FACS analysis showing the IgA rescue efficiency by WT^R and $Med12^R$ deletion mutants in $Med12^{KD}$ CH12F3-2A cells. Mock contains empty backbone vector. (**C**) LM-PCR assay detecting the DNA break in WT^R and corresponding domain deleted constructs, followed by Southern blot with the 5′-Sμ–specific probe. GAPDH was used as internal control. The triangles indicate a 3× dilution in the DNA amount. Right: The ImageJ analysis showing the quantitative band intensities in the respective samples. (**D**) 3C-PCR analysis in WT^R and indicated Med12 deletion constructs in $Med12^{KD}$ cells. GAPDH PCR of the cross-linked DNA sample served as a loading control. Right: The ImageJ analysis showing the quantification of the band intensities in respective samples. (**E**) The schematic showing the overview of experiment. The Med12 LS and PQL domains tagged with V5 and/or Flag were cotransfected in human embryonic kidney (HEK) 293T cells as depicted (right) and probed as indicated antibodies. (**F**) Top: Schematic representation of the WT^R Med12 protein and its associated various disease linked point mutations scattered over LS and PQL domains. The different color code corresponds to linked disease. Bottom: The IgA rescue efficiency in disease linked Med12 mutations in $Med12^{KD}$ CH12F3-2A cells. (**G**) LM-PCR assay for estimation AID-induced DNA break rescue in WT^R and corresponding disease-linked CSR-defective mutants in $Med12^{KD}$ cells. Right: The ImageJ analysis showing the quantification of the band intensities in respective samples. The result summarizes the means ± SD of three independents experiments, and the statistical significance was determined by two-tailed Student's *t* test ($P > 0.05$). XLID, X-linked intellectual disability.

nor ΔPQL^R transfection restores Sμ-Sα or Eμ-Sα interaction in $Med12^{KD}$ cells. However, we find that cotransfection of both ΔLS^R and ΔPQL^R rescues Sμ-Sα and Eμ-Sα interactions, suggesting that both the LS and PQL domain are required for synapse formation.

As only cotransfection of ΔLS^R and ΔPQL^R restored DNA break and synapse, it suggested a functional cross-complementation by the two domains, presumably through their interaction, if Med12 forms a homodimer or multimer. To examine the possibility, we performed coimmunoprecipitation (Co-IP) of differentially epitope-tagged (V5 and Flag and vice versa) LS and PQL domains, as depicted in Fig. 2E. The Co-IP result suggests that the LS and PQL domains form homodimers and also interact with each other. Moreover, the complex also pulled down p300

histone acetyltransferase (HAT), an essential interacting partner of Med12 for its function in CSR, as we revealed in the subsequent sections.

Furthermore, to examine whether Med12 mutations observed in human disease have CSR defects, we tested several reported point mutations across multiple Med12 protein domains (table S1). Because the LS domain is associated with XLID, we also included two previously unknown LS domain mutations (R1138H and R1463C) that were generated during the site-directed mutagenesis process. We find that mutations in the LS (R521H, R1138H, L1224F, and R1463C) and PQL (H1729N, R1862K, and R1899K) domains show diminished CSR activity (Fig. 2F and table S1). Point mutants that induced significant CSR defects (R1138H, R1463C, R1862K, and R1899K) were further examined for their ability to promote AID-induced DNA DSBs. LM-PCR assays show that impaired DNA DSB formation in Med12^{KD} cells can be restored by complementation with PQL domain mutants (R1862K and R1899K) but not by LS domain mutants (R1138H and R1463C) (Fig. 2G). Despite promoting DNA DSBs as efficiently as WT Med12, PQL mutants were CSR defective (Fig. 2F and table S1), likely because of their recombination defects. Together, we suggest that Med12 regulates two distinct steps of CSR, namely, AID-induced DNA DSBs using its LS domain and S region synapse formation using its PQL domain.

The transcription regulatory kinase module of Med12 is dispensable for CSR

The N-terminal L domain of Med12 plays an important role in transcriptional regulation through its interaction with the kinase module and the core Mediator (*20*). The Mediator kinase module is composed of Med12, cyclin C, Cdk8/Cdk19, and Med13. This kinase module reversibly interacts with the core Mediator through Med13 and contributes to gene expression regulation (Fig. 3A) (*33*). As Med12 stimulates Cdk8/19 kinase activity through cyclin C–dependent interaction, loss of Med12 or a defect at the N terminus disrupts kinase complex formation, resulting in gene expression defects (*33*). To test the requirement of the kinase module and the core Mediator for CSR, we treated CH12F3-2A cells by cortistatin A (CA), a potent pharmacological inhibitor of Cdk8 and its paralog Cdk19 (*34*). Unexpectedly, CA treatment (100 or 250 nM) did not show any inhibitory effect on CSR compared to dimethyl sulfoxide (DMSO) control (Fig. 3B and fig. S2A). We confirmed the effectiveness of CA treatment (250 nM) by examining the expression of kinase module–regulated and CA-sensitive genes, namely, Egr1, Atf1, and Atf7 (Fig. 3C and fig. S2B) (*35*). In addition, the depletion of Cdk8 by siRNA had no significant effect on CSR (Fig. 3D and fig. S2C), despite Cdk8 mRNA being efficiently down-regulated by three independent siCdk8s (Fig. 3E and fig. S2C).

To further investigate kinase module–independent functions of Med12 in CSR, we modeled three Med12 mutations (L36R, Q43P, and G44S) that are associated with UL (Fig. 3F) (*36*). These mutations disrupt Med12 interaction with cyclin C and Cdk8/Cdk19. Notably, each single mutation alone was sufficient to abolish the kinase module–dependent functions of Med12 (*36*). We confirmed the loss of Cdk8 interaction in these Med12 mutants by Co-IP (Fig. 3F). Furthermore, all three mutants fully restored CSR activity (Fig. 3G). These results are consistent with the insensitivity of CSR to CA treatment and Cdk8 depletion (Fig. 3, B and D) and further suggest kinase module–independent functions of Med12 in CSR (Fig. 3J).

Furthermore, to test the requirement of core Mediator in CSR, we knocked down Med13 and its paralog Med13like (Med13L), which is required for kinase module interaction with the core Mediator (Fig. 3A). Med13 and Med13L were depleted up to 70 to 80% by siMed13-1 and siMed13L-3, respectively. However, CSR was not significantly affected following Med13 or Med13L depletion (Fig. 3, H and I, and fig. S2, D and E). We observed a slight decrease in CSR by siMed13-2/siMed13-3 that we deemed as nonspecific, as it did not correlate with KD efficiency (fig. S2D). Together, we conclude from these multiple lines of evidence that Med12 promotes CSR independently of its kinase module and the core Mediator (Fig. 3J).

Med12-p300 complex regulates CSR through 3′RR enhancer activation

Previous reports have largely focused on the kinase module–mediated functions of Med12, leaving the kinase module– or core Mediator–independent functions of Med12 largely unknown. A recent report suggests that Med12 regulates hematopoietic stem cell–specific super-enhancers in cooperation with the HAT p300 and independent of the Med12 kinase module (*22*). From this, we asked whether Med12 might analogously activate the IgH 3′RR.

To test this hypothesis, we first examined whether deposition of the hallmark enhancer marker, H3K27ac, at the IgH 3′RR super-enhancer was dependent on Med12 and p300. We find that depletion of either Med12 or p300 markedly reduces H3K27ac deposition across the enhancer clusters (hs3a, hs1.2, hs3b, hs4, hs5, hs6, and hs7) in 3′RR (Fig. 4, A to C, and fig. S3A). Because p300 is a key acetyltransferase that catalyzes H3K27 acetylation at enhancers, we tested whether p300 recruitment at the IgH 3′RR was dependent on Med12. Med12 depletion significantly reduced p300 localization at the 3′RR enhancer (Fig. 4D). In support of this finding, co-IP analysis confirms the interaction between Med12 and p300 (fig. S3B). Furthermore, functional depletion of p300, either by siRNA or HAT catalytic inhibition by C646 inhibitor (p300^{In}), led to CSR impairment (Fig. 4E and fig. S3, A and C) and decreased H3K27ac at the enhancer.

To confirm whether p300 loss recapitulates the Med12 loss, we investigated the three essential steps for CSR: (i) Switch GLT, (ii) DNA DSB formation, and (iii) S-S synapse formation. Unexpectedly, p300 depletion decreased S region DSBs as well as interactions between Sμ-Sα and Eμ-3′RR (fig. S3, E to G), similar to the defects observed following Med12 depletion (Fig. 1, D and F). In addition, similar to Med12^{KD} (Fig. 1C), transcription of μGLT and αGLT were not perturbed following p300 depletion (fig. S3H). However, p300 KD or its catalytic inhibition decreased DSB associated γH2AX formation in the S region (Fig. 4F and fig. S3D). Given this observation, we examined H3K4me3 marks in the S region, as they are essential for AID-induced DNA DSBs (*37*–*39*). Depletion of Med12 or p300 resulted in a significant loss of H3K4me3 at the S region (Fig. 4, G and H). We observed a similar loss of H3K4me3 from both the Sμ and Sα regions following p300 inhibition (fig. S3D). Co-IP experiments also showed that the Med12-p300 complex contains critical components involved in histone lysine 4 methylation, such as Ash2 and Wdr5 (fig. S3B). Loss of either Ash2 or Wdr5 also significantly reduced S region H3K4me3 and γH2AX formation, resulting in impaired AID-induced DSB and CSR (*38*).

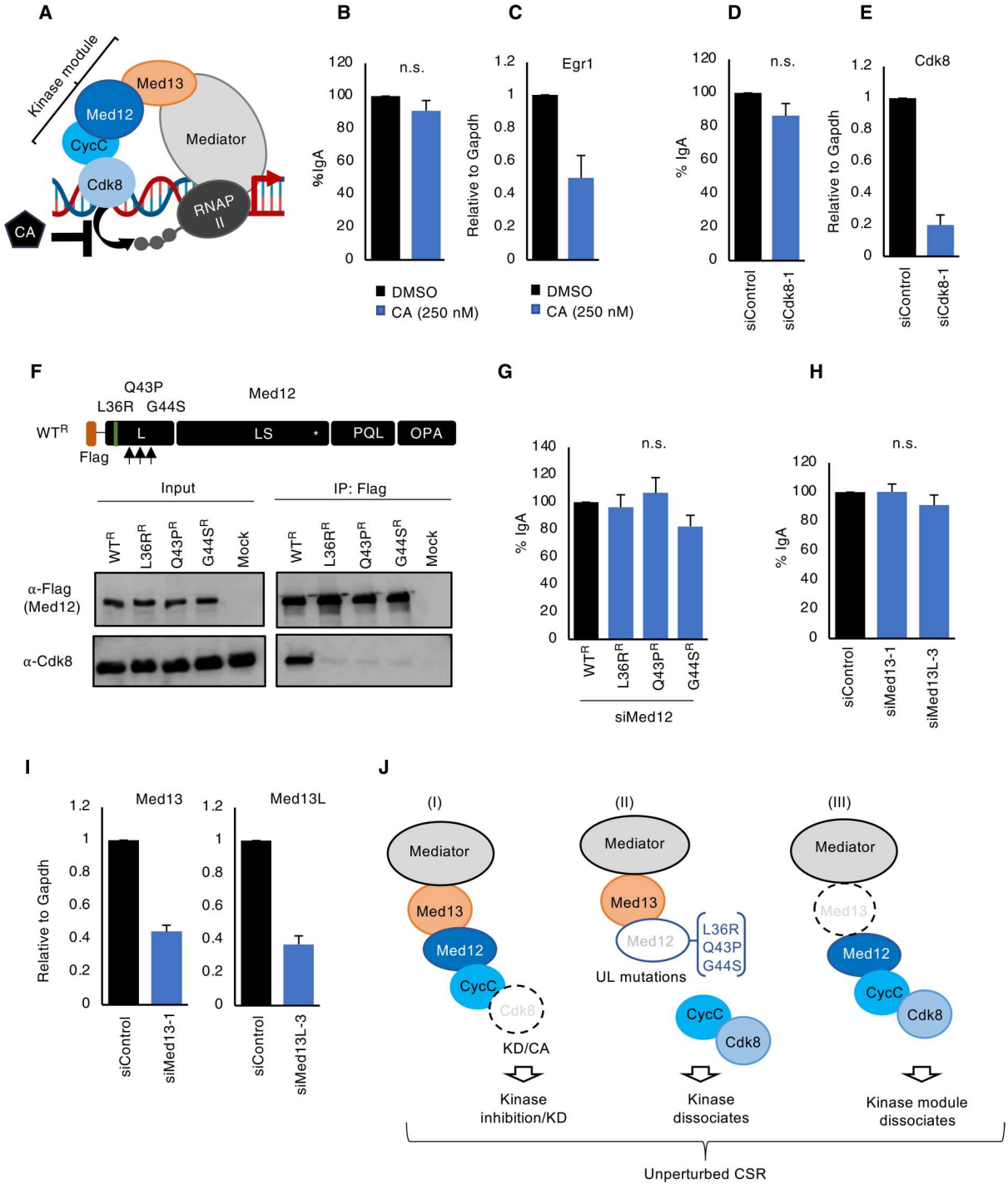

Fig. 3. Med12 does not require kinase and core Mediator complex for CSR. (**A**) Schematic representation depicting the Med12 kinase module and core Mediator function involved in transcription regulation. Med12 kinase module consists of four proteins (Med12, Med13, CcyC, and cdk8), and Med13 act as an anchor and connects the kinase module to the core Mediator complex. CA inhibits the Med12 kinase activity by binding to Cdk8 and inhibits the RNAPII phosphorylation and gene transcription. (**B**) The bar plot showing the effect of CA on IgA switching. (**C**) Egr1 transcript abundance was estimated by RT-qPCR and served as positive control. (**D**) The bar plot showing the effect of Cdk8 knockdown (KD) on IgA switching and (**E**) corresponding RT-qPCR analysis. The values have been normalized to endogenous GAPDH. (**F**) Top: Schematic representation of UL-linked point mutations found on Med12. Bottom: The HEK293T cells were transfected with indicated Med12 constructs, and later, flag IP was performed. Mock shows untransfected cells. (**G**) The bar plot showing the effect of IgA complementation by UL-linked Med12 point mutations in siMed12 CH12F3-2A cells. (**H** and **I**) The effect of Med13 and Med13L KD on IgA switching. The CH12F3-2A cells were transfected with either siMed13 or siMed13L and CIT (+) for 24 hours and analyzed by FACS. The samples have been collected and processed for RT-qPCR analysis and plotted after the GAPDH normalization. (**J**) The schematic showing the stepwise dissection of the kinase domain and their components requirement for CSR. The result summarizes the means ± SD of three independents experiments, and the statistical significance was determined by two-tailed Student's *t* test ($P > 0.05$); n.s. indicates insignificant difference.

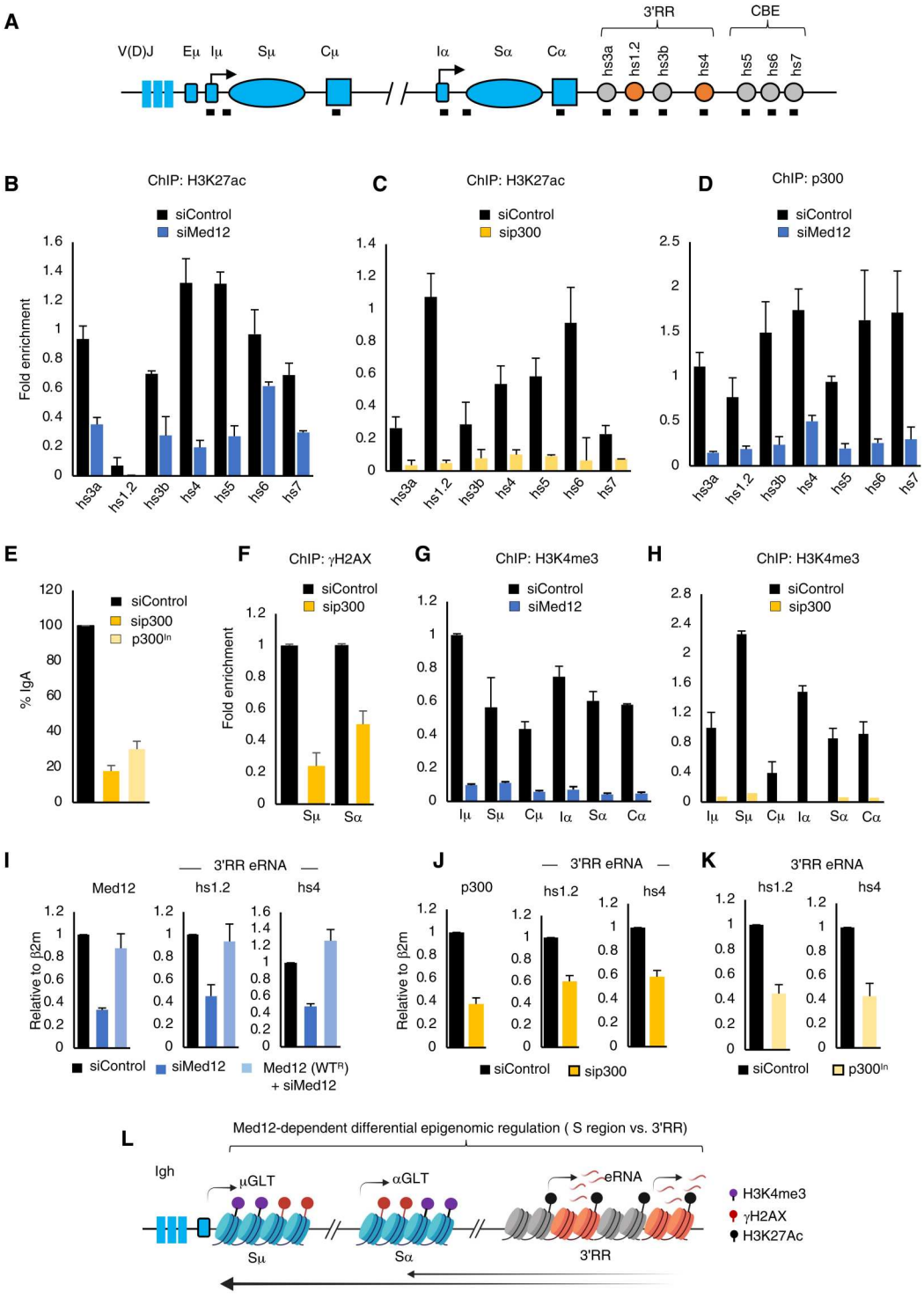

Fig. 4. 3′RR enhancer activation by Med12-p300 complex is required for AID-induced DNA break and S-S synapse. (**A**) Schematic showing the different regions present at the IgH locus; the black bar showing the position of the primers used for ChIP-qPCR amplification. (**B** to **D**) The ChIP-qPCR showing the enrichment in control and Med12 and/or p300 KD cells using the indicated antibodies. The values were normalized to the DNA input signals, followed by the maximum value in each dataset. (**E**) The bar plot showing p300 KD by siRNA and inhibition of p300 histone acetyltransferase (HAT) ($p300^{In}$) activity by C646 (5 nM) and their effect on CSR. The samples were transfected and analyzed as mentioned before. (**F** to **H**) The ChIP-qPCR showing the relative enrichment in control and KD cells as indicated. The antibody used for ChIP is indicated on each panel. (**I** to **K**) The RT-qPCR data showing the effect of Med12 and p300 KD or $p300^{In}$ on indicated transcripts relative to control. The data were normalized with endogenous β2m abundance. (**L**) Schematic showing the role of Med12-dependent differential epigenomic regulation at S and 3′RR regions. We propose that Med12 activates the 3′RR enhancer through p300, which marks H3 histone acetylation (black boll). The enhancer RNA (eRNA) produced from the activated enhancers regulates the AID-induced DNA break formation by regulating the histone marks γH2AX (red boll) and H3K4me3 (purple boll) at S regions. The result summarizes the means ± SD of three independents experiments, and the statistical significance was determined by two-tailed Student's *t* test ($P > 0.05$).

In summary, 3′RR activation through the coordinated activity of Med12 and p300 appears to be crucial for both S region chromatin remodeling and long-range S-S synapse formation. To further investigate this hypothesis, we tested whether transcription of noncoding eRNAs, another hallmark of active enhancers, was also dependent on Med12 and/or p300. We find that eRNA transcription from hs1.2 and hs4 is decreased by Med12 depletion and elevated by Med12 overexpression in $Med12^{KD}$ cells (Fig. 4I). Similarly, p300 depletion or HAT activity inhibition reduces 3′RR eRNA expression (Fig. 4, J and K), suggesting that 3′RR enhancer activation is dependent on Med12 and/or p300. We conclude that Med12 plays a crucial role in recruiting p300 to the 3′RR for enhancer activation and epigenomic modulation in the S region, both of which are essential for efficient CSR (Fig. 4L).

Rescue of Med12 deficiency by CRISPR-dCas9–mediated 3′RR activation

We hypothesized that the loss of 3′RR activation is the underlying cause of CSR impairment following Med12 deficiency. From this, we tested whether CSR can be restored by enforced enhancer activation using a CRISPR–dead Cas9 (dCas9)–based enhancer epigenetic remodeling system (*40*). We used a hs1.2 and/or hs4 targeting dCas9 coupled to the core HAT domain of p300 (dCas9-p300^{C}) that can catalyze H3K27 acetylation at the 3′RR enhancer (Fig. 5A) (*41*). We selected the two hypersensitive sites, hs1.2 and hs4, for targeting in CH12F3-2A, as their deletion significantly impairs CSR in mouse models (*42*, *43*).

Transfection of dCas9-p300^{C}, together with hs-specific small guide RNA (sgRNA) in Med12^{KD} cells, restored enhancer activity

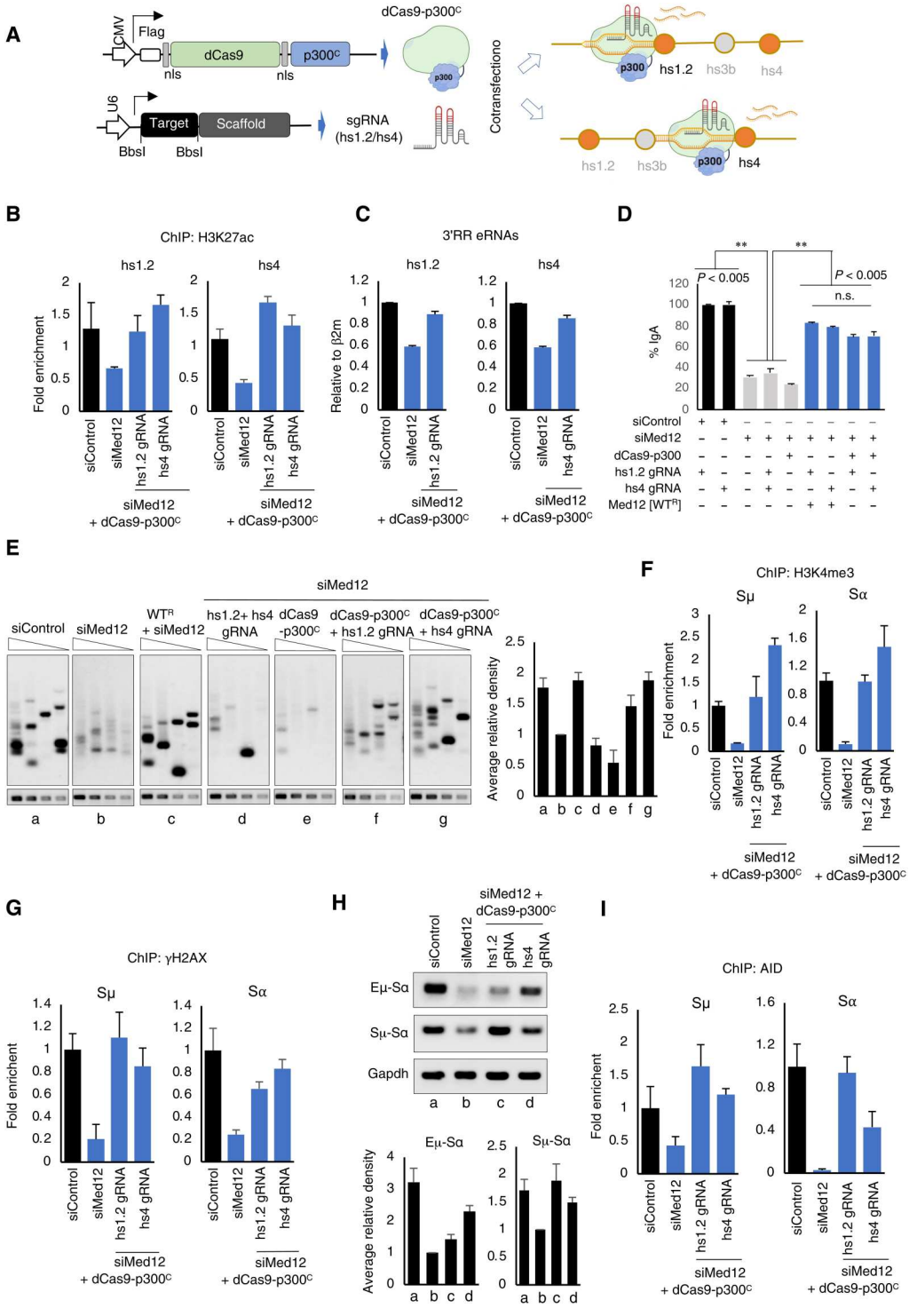

Fig. 5. Enhancer targeting CRISPR epigenetic remodeler activates the 3′RR transcription and fully complemented Med12 deficiency. (**A**) The constructs showing the dead Cas9 (dCas9) fused with p300core HAT domain (dCas9-p300^{C}) and expressed from cytomegalovirus (CMV) promoter. The small guide RNA (sgRNA) designed for hs1.2 and hs4 enhancers were expressed from the U6 promoter. The co-transfection of dCas9-p300^{C} and either sgRNAs (hs1.2/hs4) in CH12-F3-2A cells showing site-specific enhancer activation at 3′RR. (**B**) The ChIP-qPCR showing the enrichment of H3K27ac histone in dual-transfected dCas9-p300^{C} with either sgRNAs in Med12^{KD} cells. (**C**) Corresponding RT-qPCR data showing the enhancer transcripts level. (**D**) The bar plot showing the IgA rescue efficiency by dCas9-p300^{C}–mediated enhancer activation in Med12^{KD} CH12F3-2A cells. The black bar and gray bar showing the control samples. The left blue bars showing the rescue efficiency in WT^{R} cells. The right two blue bars showing the dual-transfected dCas9-p300^{C} with either sgRNAs (hs1.2 and hs4) in Med12^{KD} cells. (**E**) LM-PCR assay estimating DNA break rescue in indicated samples as described above. Right: The ImageJ analysis showing the band intensities in the respective samples. (**F** and **G**) The ChIP assay was performed using the indicated antibodies, followed by qPCR showing the enrichment at S regions in dual-transfected dCas9-p300^{C} with sgRNAs (hs1.2 and hs4) in Med12^{KD} cells. (**H**) The 3C-PCR assay showing long-range interaction (LRI) in dual-transfected dCas9-p300^{C} with Med12^{KD} cells. Bottom: The ImageJ analysis showing the band intensities in the respective samples. (**I**) The ChIP-qPCR showing the AID enrichment in dual-transfected dCas9-p300^{C} with sgRNAs in Med12^{KD} cells. The result summarizes the means ± SD of three independents experiments, and the statistical significance was determined by two-tailed Student's *t* test ($P > 0.05$).

as measured by complete recovery of H3K27ac deposition and a concomitant increase in eRNA transcription (Fig. 5, B and C). Targeting dCas9-p300^{C} to one of the hypersensitive sites is sufficient to compensate for epigenetic deficits at the other site, possibly due to their palindromic nature and sequence similarity (*44*). As expected, cotransfection of dCas9-p300^{C} and hs-sgRNA rescued the CSR defect in Med12^{KD} cells nearly as efficiently as by rescue with the WT^{R} construct (Fig. 5D; compare first two blue bars versus last two blue bars). Neither sgRNA (hs1.2/hs4) nor dCas9-p300^{C} transfection alone affected the CSR compensation in Med12^{KD} cells (Fig. 5D, gray bars).

Similarly, cotransfection of dCas9-p300^{C} and hs-sgRNA also restored S region DSB formation in Med12^{KD} cells as detected by our LM-PCR assay (Fig. 5E; compare b versus f and g). DSB signals derived from Med12^{KD} cells transfected with hs1.2 and hs4 sgRNA or dCas9-p300^{C} were considered as background (Fig. 5E, d and e). Notably, enforced activation of 3′RR in Med12^{KD} cells also restored S region H3K4me3 and γH2AX marks (Fig. 5, F and G). Transfection with dCas9-p300^{C} and hs1.2 or hs4 sgRNA also largely restored long-range interactions between Sμ-Sα/Eμ-Sα in Med12^{KD} cells (Fig. 5H).

Because AID is essential to S region DNA DSB and S-S synapse formation, we also examined how enhancer reactivation affects AID recruitment to the IgH locus, a process that has previously been reported to be 3′RR dependent (*10*, *13*). In Med12^{KD} cells, AID was reduced at S regions and was restored to control levels upon cotransfection with dCas9-p300^{C} and enhancer-targeting sgRNAs (Fig. 5I). AID has also been reported to target 3′RR and was found to be distributed across the 3′RR super-enhancer region (*45*). Furthermore, AID-induced DNA breaks at 3′RR are responsible for locus suicide recombination (LSR), a process that removes a large sequence region containing Sμ and 3′RR and leads to impaired cell survival. LSR is considered an intrinsic mechanism to regulate B cell homeostasis and for selection of antigen-specific B cells. We observed that Med12 depletion also reduces AID recruitment at 3′RR (fig. S4A). However, it remains to be determined whether Med12 and/or 3′RR eRNA also regulate LSR (*45*).

Together, our findings suggest that 3′RR activation by CRISPR–dCas9-p300^{C} compensates for CSR defects following Med12 deficiency, likely through restoring multiple epigenetic processes in the S region, including H3K4me3 formation, DNA DSB induction, and S-S synapse formation. In summary, Med12 is an indispensable chromatin remodeling factor for IgH 3′RR activation and associated CSR.

Mechanism of Med12-dependent IgH 3′RR eRNA regulation

Here, we provide evidence that Med12-dependent 3′RR eRNA transcription is critical for CSR regulation. However, several outstanding questions remain, including how Med12 is recruited to the IgH enhancer and how the enhancer activation functions of Med12 are regulated. To address these questions, we used an ER-bound enhancer (ERE) element eRNA transcription system. In this system, eRNA transcript expression is strongly and rapidly induced following estrogen exposure (*46*). Recent evidence suggests that Jmjd6, a multifunctional enzyme, regulates ERE-derived eRNA transcription by recruiting Med12 and the Carm1 complex (*47*). Jmjd6 may also be necessary for Med12 interaction with Carm1, which, in turn, methylates Med12 at multiple arginine sites to facilitate chromatin binding.

To test the involvement of the Jmjd6/Carm1 pathway in 3′RR regulation through Med12, we first confirmed the presence of Jmjd6/Carm1 at the IgH 3′RR and that this occupancy can be depleted by using siRNA against Jmjd6 (Fig. 6A). We find by chromatin IP (ChIP) analysis that Jmjd6/Carm1 occupies the 3′RR and that this occupancy is dependent on Med12 (Fig. 6B). This finding prompted us to examine whether Jmjd6/Carm1 depletion also affects CSR and 3′RR eRNA transcription. We find that depletion of Jmjd6/Carm1 reduces CSR, and eRNA transcription from both hs1.2 and hs4 and is correlated with KD efficiencies (Fig. 6, C and D). Furthermore, ChIP analysis revealed that reduced eRNA transcription in Jmjd6^{KD} cells was likely due to the loss of H3K27ac mark but not loss of Med12 at the 3′RR, as Jmjd6 depletion specifically reduced H3K27ac and p300 protein enrichment (Fig. 6, E and F). We confirmed the specificity of siJmjd6 by using an siRNA-resistant transcript (WT-jmjd6^{R}) that successfully restored the siJmjd6-mediated CSR inhibition (fig. S4D). As expected, expression of WT-Jmjd6^{R} but not the catalytically defective mutant (H187A-Jmjd6^{R}) restored CSR in Jmjd6^{KD} cells (fig. S4D), suggesting that the demethylase activity of Jmjd6 may remove repressive histone marks to preserve H3K27ac at the 3′RR. To further confirm that the observed siJmjd6-mediated CSR impairment is due to the loss of H3K27ac and eRNA at the 3′RR, we activated the enhancer by cotransfecting dCas9-p300^{C} and hs4-sgRNA. This activation fully restored the CSR defect in Jmjd6^{KD} cells (Fig. 6G), further emphasizing the importance of 3′RR activation and eRNA production for CSR.

Next, to evaluate the importance of Med12 arginine methylation in CSR and 3′RR eRNA regulation, we generated Med12 mutants (R1854K, R1871K, and R1899K) that are defective in arginine methylation by Jmjd6/Carm1 (*47*). CSR complementation assays showed that all three methylation mutants were defective in CSR at variable levels of deficiency (Fig. 6H). These CSR defects are comparable to defects previously reported in the Med12 ΔPQL mutant (Fig. 2, A and B), the Med12 domain that contains critical and additional arginine methylation sites. Notably, addition of the ΔPQL mutant was also unable to restore 3′RR eRNA transcription from both the hs1.2 and hs4 enhancers in Med12^{KD} cells (Fig. 6I). Together, we conclude that the Jmjd6/Carm1 complex is an important posttranslational regulator of Med12, which cooperates with p300 to regulate 3′RR activation and eRNA transcription and efficient CSR (Fig. 6J).

Depletion of 3′RR eRNAs perturbs enhancer function and impairs CSR

eRNAs are short transcripts that are transcribed unidirectionally or bidirectionally from enhancers (*20*). eRNAs exert a plethora of functions either in cis or trans, including regulating transcription through recruiting transcription and/or chromatin remodeling factors, regulating long-range interaction between enhancer and promoter sequences, and regulating histone modifications (*48*). At some enhancers, H3K27ac deposition and Mediator complex recruitment are dependent on eRNA production (*48*, *49*). From this, we attempted to clarify the role of 3′RR eRNAs in histone modification at the 3′RR and S region, as well as the role of 3′RR eRNAs in S region DSB, S-S synapse formation, DNA repair, and CSR.

To specifically deplete 3′RR eRNAs, we designed locked nucleic acid–modified antisense oligos (ASO1 and ASO2) targeting the hs4 enhancer. We chose hs4 because of its basal eRNA expression in CH12F3-2A cells, which is several folds higher than hs1.2 basal

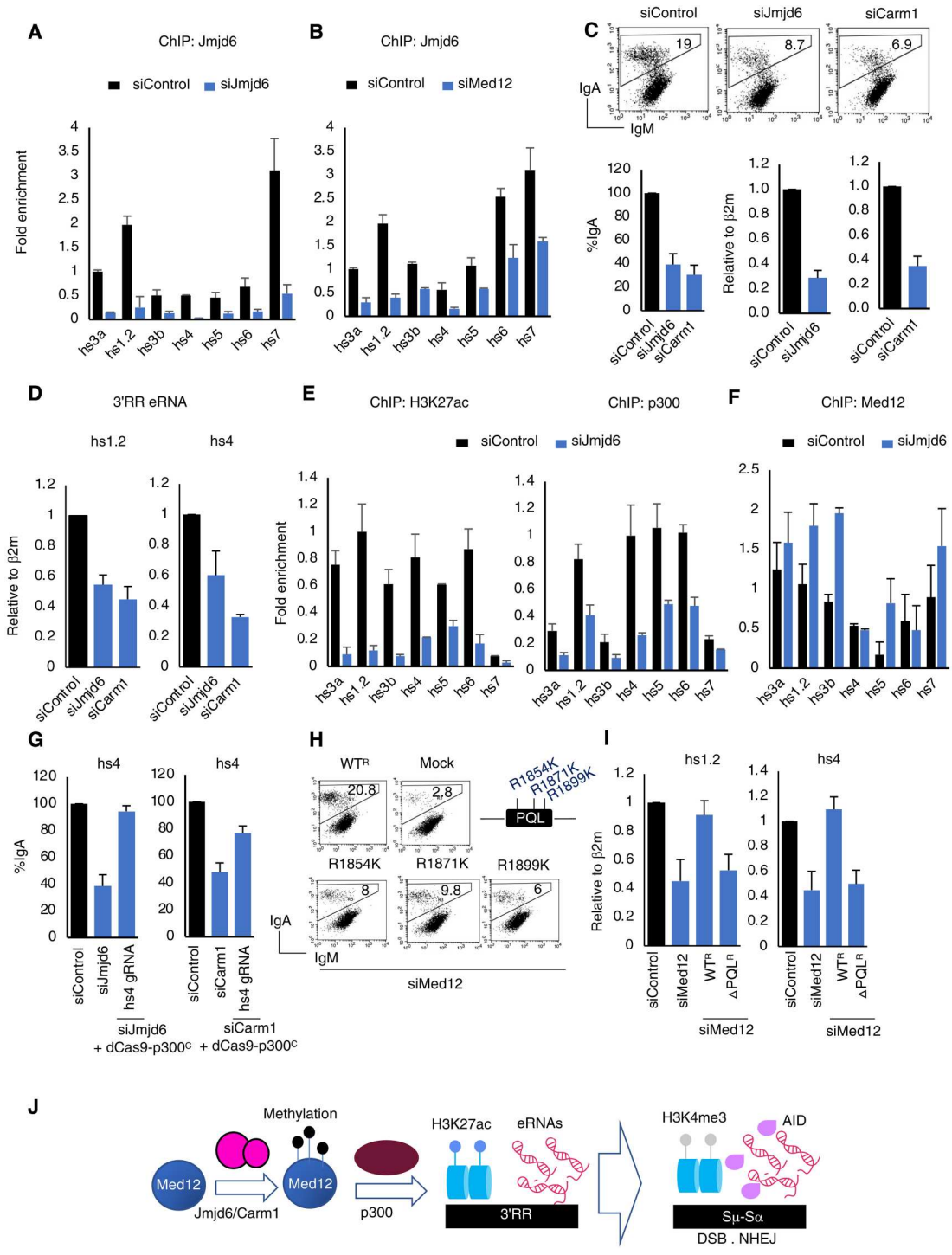

Fig. 6. Med12 methylation by Jmjd6/Carm1 initiates enhancer activation. (**A** and **B**) The ChIP-qPCR showing the occupancy of Jmjd6 at 3′RR in control and either Jmjd6- or Med12-depleted cells. (**C**) Top: The FACS data showing the effect of Jmjd6 and Carm1 KD by respective siRNAs. Bottom left: The RT-qPCR data showing the KD efficiency by respective samples, and the data were normalized with β2m abundance. (**D**) The bar plot showing the effect of Jmjd6 and Carm1 KD on 3′RR transcripts. (**E** and **F**) The ChIP assay was performed by indicated the antibodies, followed by qPCR in control and Jmjd6 KD cells. (**G**) The bar plot showing the IgA rescue efficiency in dual-transfected dCas9-p300^{C} with hs4 sgRNAs in Jmjd6 and/or Carm1 KD cells. (**H**) The FACS analysis showing the IgA rescue efficiency in methylation-defective Med12 mutants in Med12^{KD} cells. The position of the mutations at PQL domain is shown at the right. (**I**) The RT-qPCR analysis showing the rescue of hs1.2 and hs4 transcripts in WT^{R} and ΔPQL Med12 mutant in Med12^{KD} cells. (**J**) The schematic representation showing the sequential steps of Med12 workflow in CSR. Med12 is methylated by Jmjd6/Carm1 complex (magenta) at different positions (black boll). Methylation recruits p300 protein to 3′RR, which marks histone H3K27 acetylation and activate the enhancers. Activated enhancers were transcribed into eRNA, which regulates H3K4me3 at S region and recruits DNA break and repair complex for CSR. The result summarizes the means ± SD of three independents experiments and the statistical significance was determined by two-tailed Student's *t* test ($P > 0.05$). NHEJ, nonhomologous end joining.

eRNA expression (fig. S4B). Transfection of hs4-specific ASOs but not an unrelated control ASO strongly inhibited IgA switching in CH12F3-2A cells (Fig. 7A). Depletion of hs4-specific eRNAs by ASO1 and ASO2 was also confirmed by qRT-PCR (Fig. 7B). Neither μGLT nor αGLT transcript expression was affected by ASO1/ASO2 treatment (Fig. 7B). A similar level of CSR impairment by ASOs was also observed in the AIDER expressing CH12-F3-2A cell line, where CSR is induced through activation of an ER-fused AID by 4-hydroxytamoxifen (OHT) (tamoxifen) treatment (fig. S4C).

Next, we examined whether CSR defects are correlated with S region DSB by LM-PCR and ChIP assays. As expected, transfection of ASOs into CH12F3-2A cells markedly reduced S region DSB signals, as compared to control ASOs (Fig. 7C). Using the most potent ASO, we evaluated DNA breaks and damage response–associated histone marks at the S regions. We observed a severe defect in H3K4me3 deposition and γH2AX formation in ASO1-transfected

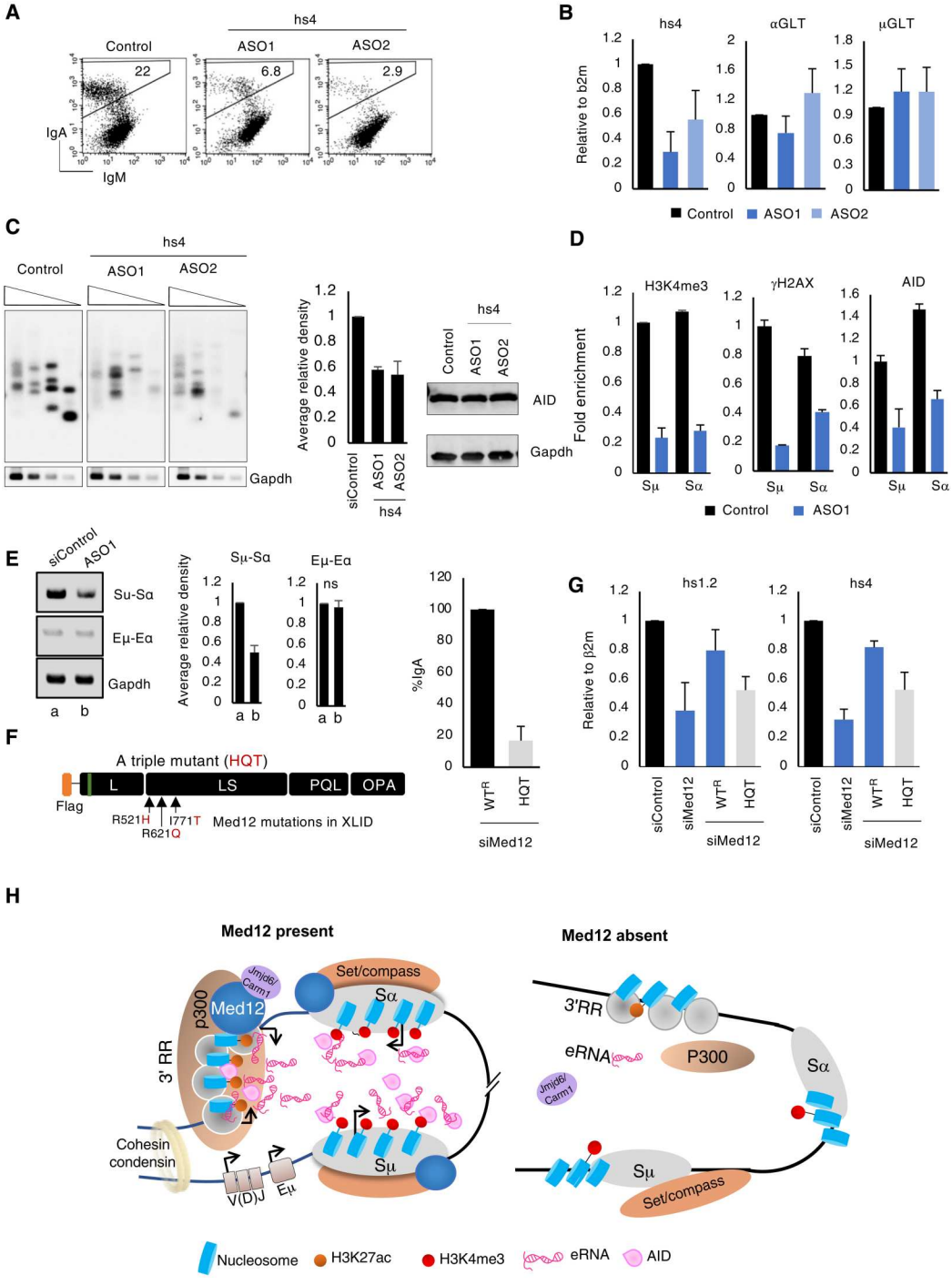

Fig. 7. 3′RR-transcribed eRNA regulates AID-induced DNA break and S-S synapsis. (**A**) FACS data showing the effect of antisense oligos (ASOs) on IgA switching. (**B**) RT-qPCR data showing the effect of ASOs on GLTs and hs4 transcripts relative to control. (**C**) Left: LM-PCR assay showing the effect of AID-induced DNA breaks in ASOs treated cells. Bottom panel shows the semi-qPCR analysis of GAPDH of respected samples as an internal control. Middle: The ImageJ analysis showing the normalized band intensities in the respective samples. Right: The Western blotting (WB) showing the effect of both ASOs on AID protein expression. (**D**) The ChIP assay was performed using the indicated antibodies, followed by qPCR showing the enrichment in control and ASO1 KD cells. (**E**) 3C assay showing the LRI in control and ASO1 KD cells. GAPDH PCR of the cross-linked DNA sample served as a loading control. (**F**) Schematic representation of Med12 protein showing the position of mutations found in nonspecific XLID disease. The IgA rescue efficiency has been determined in XLID-associated triple mutant (HQT) in Med12^{KD} cells. (**G**) The RT-qPCR showing the effect of Med12 HQT mutant on 3′RR transcription. (**H**) The proposed model showing the role of Med12 in enhancer activation. Med12 recruits p300 at 3′RR enhancers, which, in turn, catalyzes the H3K27ac histone acetylation. Med12-p300 complex initiates the enhancer activation, which transcribed into the eRNA. The eRNA produced from the 3′RR and recruits Med12, H3K4me3 methyltransferase, and DNA break complex at S regions. In the absence of Med12, p300 does not recruit to 3′RR, resulting in inactivation of enhancers and perturbed DNA break and S-S synapse formation. The result summarizes the means ± SD of three independents experiments, and the statistical significance was determined by two-tailed Student's *t* test ($P > 0.05$).

cells (Fig. 7D), which was consistent with S region DSB impairment (Fig. 7C). AID association with the IgH locus decreased following ASO1 treatment (Fig. 7D) despite AID levels remaining unchanged (Fig. 7C). Notably, in addition to impaired AID-induced S region DNA breaks, long-range Sμ and Sα interactions were also disrupted (but not Eμ-3′RR) following ASO1 transfection (Fig. 7E). It is notable that 3′RR-eRNA depletion following ASO treatment also impaired the two key steps of CSR: S region DSBs and S-S synapse formation consistent with our observations following Med12 depletion. Together, our data suggest that Med12 functions in CSR are dependent on eRNA expression from the 3′RR.

We find that the Med12 mutant with multiple XLID mutations (R521H/R621Q/I771T), which we named "HQT," shows significant CSR impairment and 3′RR eRNA transcription defects (Fig 7, F and G). Such a function has never been reported for any XLID mutations; we also find loss of the Med12 PQL domain impairs CSR and 3′RR eRNA transcription (Figs. 2B and 6I). Our findings that the LS and PQL domains of Med12 regulate CSR imply that both AID-driven DNA DSBs and S-S synapse formation require 3′RR activation and more specifically eRNA transcription.

We noticed that Med12 has intrinsically disordered regions (IDRs) across the LS and PQL domains (fig. S6A). A comparison of Predictor of Natural Disordered Regions (PONDR) analysis revealed that the feature is very similar to Med1 and Brd4 (fig. S6A). We also confirmed that Med12 is an IDR-containing protein by precipitating IDR-specific chemical (fig. S6C), biotinylated isoxazole or b-Isox, which also precipitated other known IDR-containing proteins, including Med1 and Brd4 (*50*, *51*). Because of the presence of IDRs, Med1 and Brd4 can undergo nuclear phase separation to form condensate at the enhancers (*50*, *51*). To investigate that this is the case for Med12, we similarly used the chemical 1,6-hexanediol (1,6-HD) to disrupt the Med12-eRNA complex, perturbing the phase separation. There was a clear dose-dependent inhibition of CSR and concomitant decrease of eRNA synthesis at the IgH 3′RR by the 1,6-HD treatment (fig. S6B).

We propose that IgH 3′RR-derived eRNAs drive epigenomic regulation at the IgH 3′RR enhancer and the S-region, stabilizing S-S proximity and promoting AID-induced DNA DSBs and CSR through recombination-associated condensate formation, which awaits further investigation.

DISCUSSION

Med12 and AID have functional homology for DNA DSBs and S-S synapse formation during CSR

AID is an indispensable enzyme for generating the DNA DSBs and S region synapses that are required for oriented deletional recombination during CSR (*6*, *7*, *52*). How AID regulates the mechanistically distinct processes of S region DNA DSBs and S-S synapse formation remains poorly understood (*53*). While numerous AID-interacting and noninteracting CSR regulatory factors have been identified, these factors appear to play exclusive roles in DNA break, repair, or synapse formation (*4*, *54*, *55*). Here, we show that Med12 is a previously unknown CSR cofactor that not only promotes AID-induced DNA DSBs and synapse formation but also supports DNA repair via NHEJ (Fig. 1, D to F, and fig. S1E). We find that Med12 shares with AID many of the key functional aspects that are essential for efficient CSR and, eventually, Ig gene diversity. As CSR is highly sensitive to Med12 protein levels, we consider Med12 levels to be a key rate-limiting factor for DNA DSBs and S region synapse formation. Our analysis of multiple Med12 mutations (table S1) shows that the LS and PQL domains are critical for efficient CSR (Fig. 2F) and likely have distinct yet overlapping functions. Loss of the LS, but not PQL domain, leads to severe impairment of DNA DSBs and DDR signals such as γH2AX formation in the S region (Figs. 1, D and E, and 2C). However, deletion of either domain leads to impaired S-S synapse formation and loss of AID occupancy at the IgH locus (Figs. 2D and 5I). Our cross-complementation and studies using Med12 mutants also suggests that, while the LS domain is crucial for AID-induced DNA DSBs, both the LS and PQL domains are necessary for S-S and Eμ-3′RR interaction (Figs. 1F and 2D). The LS and PQL domains are likely involved in Med12 dimerization or multimerization (Fig. 2E) that associates with the eRNA-protein complex to form local enhanceosome (*50*) or condensate (fig. S6B).

Med12-dependent IgH 3′RR super-enhancer activation is central to CSR

Consistent with Med12′s function in IgH locus DNA DSBs and long-range chromatin looping, we find Med12 enrichment at the Eμ, Sμ, Sα, and 3′RR super-enhancer regions (fig. S5, A to C) (*56*). However, Mediator is a 30-subunit megadalton complex with four submodules, including the Med12-containing kinase module that reversibly interacts with the core Mediator for transcriptional regulation (*20*). At the IgH locus, Med12 functions in CSR appear independent of its kinase function, as CSR was refractory to CDK8 depletion or catalytic inhibition of the CDK8 kinase. These findings are also consistent with competent CSR observed in Med12 mutants that are defective in CDK8 activation (Fig. 3, F and G). Similarly, depletion of Med13/Med13L, the essential bridging component between core Mediator and the kinase module, does not affect CSR (Fig. 3H). While other associations may still exist, these kinase-independent functions of Med12 are reminiscent of Med12 functions in human pluripotent stem cells (HPSC) homeostasis (*22*), where Med12 helps regulate cell lineage–specific super-enhancers in a kinase-independent manner.

H3K27ac and H3K4me1 on enhancer chromatin distinguish transcriptionally active enhancers from inactive and paused enhancers (*57*). Priming of enhancer activation occurs through the binding of pioneering TFs and subsequent loading of other TFs, co-activators, and RNAPII to generate eRNA from super-enhancers (*58*). Consistent with previous reports, our work suggests that Med12 maintains IgH 3′RR super-enhancer activation through p300, as Med12 depletion results in p300 recruitment defects, impaired H3K27ac deposition, and 3′RR eRNA transcription (Fig. 4, C, D, I, and J). Here, we used multiple lines of evidence to demonstrate the importance of IgH enhancer activation for CSR. These lines of evidence included (i) a Med12 deficiency complementation for CSR by CRISPR-dCas9 enhancer activation system that restored H3K27ac signature and eRNA synthesis at 3′RR (Fig. 5, B and C), (ii) recapitulating 3′RR inactivation and CSR defects observed in Med12 deficiency by p300 depletion or inhibition (Fig. 4, C, J, and K), and (iii) degradation of 3′RR eRNAs by ASO targeting shows strong CSR impairment, as well as impaired S region DNA DSBs, reduced long-range interactions, and reduced AID recruitment to the IgH locus (Fig. 7, C to E). We obtained similar results when eRNA processing was interrupted by depleting the catalytic subunit of the integrator complex (IntS11 and IntS13) (fig.

S4E), which regulates the length and production of eRNAs (*59*). Consistent with these findings, we also find enrichment of IntS11 and IntS13 at the 3′RR enhancer after stimulation with CIT for CSR (fig. S4F).

The requirement of the 3′RR super-enhancer in CSR has been well documented by numerous elegant studies in mice models and ex vivo system (*9*, *13*). However, there remains minimal information regarding the mechanisms of 3′RR activation and how this activation affects AID-induced CSR events. Recently, Zymnd8 that recognizes various histone modifications was shown to reduce RNAPII loading at the IgH super-enhancer and reduce enhancer transcription (*60*). Conversely, RNAPII elongation factor Spt5 may regulate 3′RR transcription by regulating RNAPII pause release (*61*). Transcription elongation factor (SPT5) deficiency does not disrupt Med12 or H3K27ac occupancy at the 3′RR, and a CRISPR-dCas9–VPR transcriptional activation system can rescue enhancer transcription defects but not CSR. This is likely due to Spt5 being required for AID expression and recruitment (*61*, *62*). However, we find that complementation of Med12 deficiency strictly requires an enhancer-activating CRISPR–dCas9-p300^{C} system, which restores H3K27ac marks at the 3′RR and restores eRNA transcription and CSR (Fig. 5, C and D). In conclusion, our results are consistent with Spt5 and Zymnd8 functioning downstream of enhancer activation by Med12.

Med12 and 3′RR eRNA-dependent epigenomic and conformational regulation

Promoters of actively transcribed gene loci are generally enriched with H3K4me3, a signature mark of accessible chromatin (*63*). However, at the IgH locus, actively transcribed I promoters and downstream S recombination regions are highly enriched with H3K4me3 (*64*–*66*). Down-regulation of IgH locus–specific H3K4me3 is associated with various CSR-associated defects, including impaired AID-induced S region DNA DSBs and impaired Ig isotype–specific transcription in primary B cells (*37*, *38*, *67*). Our work here is consistent with other studies, suggesting that the combinatorial histone code, including H3K4me3, facilitates DNA DSB complex formation at the S region (*37*, *38*, *68*). One of our notable findings is that Med12 deficiency causes strong down-modulation of H3K4me3 and AID-induced S region DNA DSBs. Because Med12 is in a complex with H3K4me3 writing machinery, loss of Med12 in S regions may perturb H3K4me3 complex activity, leading to impaired AID-induced DNA DSBs. Within this process, we suspect that 3′RR activation plays a critical role, as p300 depletion (or 3′RR inactivation) leads H3K4me3-impaired deposition and DNA DSB formation at S regions (Fig. 4, H and F). This hypothesis is consistent with our finding that 3′RR activation by CRISPR–dCas9-p300 system can fully restore defects caused by Med12 depletion.

Depletion of 3′RR eRNAs, the activation markers of the IgH super-enhancer, phenocopied the DNA DSB and S-S synapse formation defects observed in Med12, p300, and AID deficiency (Fig. 7, C to E). This result suggests a direct and unique role of 3′RR eRNAs in CSR regulation. We have shown that 3′RR eRNAs can bind Med12, Wdr5, Rad21, and AID (fig. S5D); and their depletion impairs recruitment of Med12, H3K4me3, and AID occupancy at S region, leading to DNA DSB and S-S synapse formation defects (Fig. 7D and fig. S5C), Notably, 3′RR eRNA depletion did not affect Med12 or H3K27ac occupancy at the 3′RR (fig. S5B), suggesting that these eRNAs predominantly contribute to CSR in a trans-manner, possibly functioning in the S regions. Consistent with this hypothesis, S region DNA DSBs and long-range Sμ-Sα but not Eμ-3′RR interactions are affected by 3′RR eRNA depletion. However, Med12 depletion leads to disruption of both chromatin loops, Sμ-Sα and Eμ-3′RR interactions (Fig. 1F), suggesting that Med12 is an essential constituent of both Sμ-Sα and Eμ-3′RR chromatin conformations. While basal levels of Med12 and 3′RR eRNAs are likely sufficient to confer Eμ-3′RR chromatin architecture, CSR induction may stabilize it further through Med12 enrichment and increased eRNA transcription. eRNA transcripts also may help Med12, AID, and other essential components localize to recombining S regions for S-S synapse formation.

Involvement of 3′RR eRNAs in CSR-specific condensate formation

Recent studies have shown super-enhancers exist as phase-separated condensates, defined as a three-dimensional reservoir holding large-scale regulatory factors and RNAs (*50*, *51*). Associated eRNAs have been implicated in stimulus-dependent (e.g., E2/epidermal growth factor) (*59*, *69*) dynamic phase separation during enhancer-promoter looping where they interact with many factors present in super-enhancers, including Med1, cohesins, YY1, p300/CBP, and BRD4 (*48*, *70*). Depletion of eRNAs from associated enhancers affected either the recruitment or function of the chromatin conformation regulatory factor, leading to disruption of enhancer-promoter chromatin looping and/or enhanceosome formation (*50*, *51*, *70*). Our work also shows that depletion of 3′RR eRNA significantly affects recruitment of Med12, AID, and possibly still unknown components to the S region. PONDR analysis (fig. S6A) suggests that Med12 has IDRs, as observed in Med1 and Brd4, both of which promote enhancer condensate formation. We also confirm that Med12, like Med1 and Brd4, can be precipitated by IDR-specific chemical b-Isox (fig. S6C) (*71*). In addition, eRNA transcription and CSR are both sensitive to 1,6-HD treatment, a known method for perturbing eRNA-dependent enhancer ribonucleoprotein complex formation and chromatin architecture (fig. S6B) (*50*).

From this, we suspect that 3′RR-derived eRNAs can act as a matrix or recruiting medium so DNA break–recombination complexes can assemble locally. While some of these defects have been previously observed in a 3′RR mouse model, the underlying mechanisms remain unclear. Our work here provides a plausible explanation for how enhancer activation and transcription can coordinate two seemingly dissimilar processes simultaneously, AID-induced DNA DSBs and S-S synapse formation.

Implications for Med12 and dysregulated CSR in XLID syndrome

Here, we have shown that mutations located near the N terminus of Med12 and those affecting Med12 kinase module (*36*) functions do not affect CSR. Conversely, several LS domain– and PQL domain–associated Med12 mutations show significant impairments in CSR (table S1). Both atypical and FG-type XLID mutations showed a marked impairment of CSR with impaired 3′RR activation/transcription (Fig. 7, F and G). It remains unknown whether patients with these XLID mutations (*72*, *73*) display mild to moderate B cell abnormalities or have Ig deficiency. Our work here suggests that the LS and PQL domains of Med12 both coordinate regulation

of eRNAs (Figs. 6I and 7G), the markers of active 3′RR super-enhancers. Although Med12 mutations have been linked to various cancer types and congenital disorders with intellectual disability, the underlying functional defects and mechanisms of these disorders remains poorly understood (table S1) (*25*). Defined and coordinated regulation of super-enhancers is essential for cell lineage and cell identity (*22*, *74*, *75*). From this, it is conceivable that Med12 defects lead to dysregulation of normal or cell lineage–specific super-enhancer functions, which ultimately give rise to neurologic disorders and/or tumors (*74*, *76*). Furthermore, many neurodevelopmental and/or intellectually disability genes are linked to DNA damage repair and the NHEJ pathway (*77*, *78*). Because NHEJ pathway is essential for both V(D)J and CSR, DNA repair defects are often a common cause of both neuronal and B cell defects. We show that Med12 deficiency may impair NHEJ; however, additional work will be needed to determine the mechanism.

Methylated Med12 initiates enhancer activation

It remains unclear how Med12 coordinates these molecular activities. It is possible that Med12's functions in CSR are regulated by interacting with other ncRNAs, specifically eRNAs and long noncoding RNAs (unpublished) and/or through arginine C-terminal methylation to regulate protein-protein or protein-RNA interactions. Carm1 methylates multiple arginine residues at the C terminus of the Med12 PQL domain. Carm1-dependent Med12 methylation sensitizes breast cancer cells to chemotherapy, and mutations at these methylation sites impair Med12 binding at the p21 locus (*27*). Recent work has shown Jmjd6 regulates Med12 methylation through Carm1, which promotes Med12 binding to estrogen receptors alpha (ERa)-bound active enhancers and regulates Med12 function (*47*). Our results partially support this model, as we find that depletion of the demethylation/methylation complex (Jmjd6/Carm1) also reduces eRNA transcription and CSR (Fig. 6, C and D). We find that Med12 is required for recruiting the Jmjd6/Carm1 complex to the IgH 3′RR locus, while Jmjd6/Carm1 is dispensable for Med12 recruitment (Fig. 6F). Furthermore, depletion of the demethylase Jmjd6 results in failures of enhancer activation (Fig. 6E). From this, we suspect that the methylation status of Med12 is crucial for enhancer activation (possibly through methylation-dependent recruitment of other coactivators/histone modifiers such as p300) to the IgH 3′RR locus, while methylation status does not affect Med12 chromatin binding. This hypothesis is strongly supported by evidence that Carm1 methylates Med12 at R1899, which is then recognized by coactivator TDRD3, leading to further interactions with activating ncRNAs for estrogen-regulated gene transcription (*26*). Crucially, we find that R1899 mutant Med12 also has diminished CSR activity (Fig. 2F). We did not find any significant difference in eRNA transcription in individual Med12 methylation defective mutants, whereas deletion of the entire PQL domain of Med12 leads to defective eRNA regulation (Fig. 6I), suggesting that combinatorial methylation is likely required for enhancer activation, a conclusion that is consistent with a previously published report (*47*).

MATERIALS AND METHODS

Cell culture, siRNA transfection, and CSR

For CSR, a derivative of mouse B cell lymphoma line (CH12F3-2A) expressing Bcl2 was used throughout the study (*29*) unless stated. Cells were cultured and maintained in RPMI 1640 supplemented with glutamine, NCTC, fetal bovine serum (10%), β-mercaptoethanol, and penicillin/streptomycin. For KD experiments, the Silencer/Stealth siRNA or control (low GC) oligonucleotides were purchase from Thermo Fisher Scientific, MA, USA, and the ASO (control or target) were purchased from QIAGEN and were introduced into the cells using the Nucleofector 96-well electroporation system (Lonza, Switzerland) as described by the manufacturer's instructions. After the transfection, the cells were cultured for 24 hours, then were stimulated by CIT cocktail (*29*) (anti-CD40L, IL-4, and TGF-β) or OHT (1 mM) for AIDER cells to induce IgM to IgA isotype switching, and cultured for another 24 to 48 hours before collection. The surface expression of IgM and IgA was examined by staining the cells with fluorescein isothiocyanate–conjugated anti-mouse IgM (eBioscience) and PE-conjugated anti-mouse IgA (eBioscience). Propidium iodide staining was included to stain the dead cells. The fluorescence-activated cell sorting (FACS) analysis was performed with a BD FACSCalibur instrument, and the data were analyzed by CellQuest software (BD Biosciences). The sequences of siRNA oligos are shown in table S2.

Plasmids

The mouse Med12 (NM_021521) cDNA was obtained by reverse transcription PCR (RT-PCR) of RNA isolated from CH12F3-2A cells and cloned into the *Asi*SI/*Mlu*I (Takara) sites of the pCMV6-Entry Mammalian Expression vector (OriGene, PS100001). The 3xFlag epitope was fused at the N-terminal of Med12 during the RT-PCR to express 3xFlag-Med12 WT construct. To generate siMed12-resistant Med12 transcripts (WT^R-Med12), the siMed12 targeting sequence (CCAUCUACUGUAACGUGGA) was modified (to CGATATATTGCAATGTAGA) without altering the encoded amino acids. WT^R-Med12 construct was further used for the deletion or point mutagenesis using the Q5 Site-Directed Mutagenesis Kit (New England Biolabs, E0554) according to the manufacturer's instructions. The LS and PQL domains of Med12 were PCR amplified using the WT^R-Med12 construct. The V5 tag was PCR amplified from Med12-pLX307 (Addgene, no. 98350) and fused to C-terminals of each domain using In-Fusion HD Cloning Kit (Takara). The primer sequence has been provided in table S2.

The mouse Jmjd6 (NM_001363363) cDNA was obtained as described above and cloned into the Hind III/Bam HI (Takara) sites of the pCMV10 vector. The 3xFlag epitope was tagged at N-terminal. To generate siJmjd6-resistant Jmjd6 transcripts (Jmjd6-WT^R), the siJmjd6 targeting sequence is modified by multiple mutageneses without altering the amino acid code. The primers sequence has been provided in the table S2.

Western blotting

For immunoblotting, total cell lysate was prepared by lysing 2×10^6 cells by the RiboCluster Profiler Kit (MBL, RN1001) supplemented with EDTA-free protease inhibitor cocktail (Roche) and ribonuclease (RNase) inhibitor (Sigma-Aldrich). After lysis for 5 min at 4°C, cells were centrifuged (135,000*g*) for 5 min, and supernatants were collected in separate tube. The obtained clear lysate was mixed with

2× SDS sample buffer in 1:1 ratio and heated for 85°C for 15 min. The denatured samples were separated by electrophoresis in 4 to 20% SDS–polyacrylamide gel electrophoresis (PAGE) (Bio-Rad) and subjected to standard Western blot analysis.

Immunoprecipitation

For each IP, Protein G Dynabeads (Invitrogen, 1003D) were preincubated with antibody of interest (5 μg) with rotation at room temperature for 1 hour. Beads were collected and washed 2× with wash buffer provided in a RiboCluster Profiler Kit (MBL, RN1001) before overnight incubation with lysate. After the incubation, beads were washed 3×, and equal ratio of 2× SDS and wash buffer were added before gel electrophoresis. For V5 IP, agarose anti-V5 tag antibody (ab1229) was used as per the manufacturer′s instructions and processed as described above.

ChIP-qPCR

The ChIP assay was performed using the ChIP-IT Express Kit (Active Motif, 53008) according to the manufacturer′s instructions. In brief, 5×10^6 cells were fixed in the presence of 1% formaldehyde for 5 min at room temperature. The reaction was stopped by the addition of 0.125 M glycine. A soluble chromatin fraction containing fragmented DNA of 500 to 2000 base pairs was obtained after cell lysis and sonication. ChIP was performed by incubating the cleared lysate with 3 μg of antibodies. The immunoprecipitated DNA was analyzed by real-time PCR, and the data were normalized first to the amount of input and then to the maximum value in each dataset, as described previously (*38*). The ChIP antibodies and primers used are listed in table S2.

RNA IP

For RNA IP (RIP) assay, 1×10^7 cells were collected, washed with cold phosphate-buffered saline, and lysed by lysis buffer (RiboCluster Profiler Kit, MBL, RN1001) supplemented with dithiothreitol, RNase inhibitor (Sigma-Aldrich), and EDTA-free protease inhibitor cocktail (Roche) as described by the manufacturer. The subsequential RIP was performed using the Magna RIP kit (Merck Millipore, 17-700) according to the manufacturer′s instruction with slight modifications. After overnight RIP, the TRIzol (Ambion) was directly added to the washed magnetic beads containing RNAs, and the total RNA was extracted using the standard RNA isolation protocol. The purity and concentration of RNA were analyzed by NanoDrop or Agilent Bioanalyzer 2100.

RNA isolation, RT, and RT-qPCR

RNA was isolated from control or treated cells using the TRIzol (Ambion), followed by *DNase* I treatment (Sigma-Aldrich, AMPD1). One microgram of purified RNA was used as template for cDNA synthesis using SuperScript IV (Invitrogen, 18090050) with random primers (Invitrogen, N8080127). Real-time PCR (Applied Biosystems, 7900HT Fast Real-Time PCR System) was performed using SYBR Green Master Mix (Applied Biosystems) and mRNA-specific primers listed in table S2. The $2^{-\Delta\Delta Ct}$ method was used to quantify the data using either Gapdh or β2 microglobulin (β2m) housekeeping transcript for normalization.

LM-PCR and 3C assay

For double-stranded DNA break estimation, CIT (+)–stimulated 1×10^6 cells per sample were collected as described above, fixed in low-melt agarose plugs, and processed for linker ligation as described previously (*30*). Briefly, linker ligation reaction was performed overnight at 16°C, and to inactivate the reaction, samples were heated at 70°C for 10 min. Threefold serial dilutions of linker ligated DNA were amplified by KOD FX Neo polymerase (Toyobo) using an Sμ-specific primer (forward) and a linker-specific primer (reverse). To confirm the amplification of Sμ-specific DSBs, Southern blot analysis of the PCR products was performed using a DIG-labeled Sμ probe. Similarly, PCR of the GAPDH locus from each sample served as a normalization control.

The 3C assay was performed as described previously (*6*, *54*). Briefly, 7×10^6 cells were collected, washed, and cross-linked for 5 min at room temperature with 1% formaldehyde. After cross-linking, the cells were subjected to nuclear lysis. The cross-linked chromatin was digested overnight with Hind III and later ligated with T4 polymerase DNA ligase (Takara). The ligated chromatin was treated with proteinase K and reverse cross-linked; furthermore, the DNA was purified by phenol/chloroform extraction protocol. PCRs were performed using the primers described in table S2.

IgH/c-Myc translocation and NHEJ assay

For translocation assay, genomic DNA has been isolated from 48 hours of CIT-stimulated samples and was PCR amplified at IgH/c-Myc translocation junctions using the Expand Long Template PCR system as described previously (*31*). The PCR products were separated by electrophoresis on ethidium bromide containing 1% agarose gels and subjected to Southern blotting with a Myc-specific probe.

The NHEJ assay was performed as described previously (*32*). In brief, The I-*Sce*I–expressing plasmid (pCBASce) alone or with siMed12 (designed against human Med12) or control was cotransfected into NHEJ reporter cell lines using Lipofectamine 2000 (Invitrogen). Transfected cells were harvested after 48 hours for FACS analysis. The NHEJ reporter cell line H1299dA3-1 was a gift from T. Kohno at the National Cancer Center Research Institute, Tokyo. The primers and siRNAs sequence were shown in table S2.

Inhibitors

CA was a gift from M. D. Shair (Harvard University) and D. J. Taatjes (University of Colorado Boulder). The dissolved CA in DMSO was provided as a stock concentration of 1 mM and was stored at −80°C for further use. The final concentrations of 100 and 250 nM were used in the experiments. The DMSO concentrations of 0.0001 and 0.00025% (without CA) were used as a vehicle control.

The P300 HAT inhibitor, C646 (Sigma-Aldrich, 328968-36-1), was dissolved in DMSO, and the 5 μM concentration was used for related experiments. The lists of antibodies, primers, and stealth siRNAs used in this study are shown in table S2.

CRISPR and sgRNAs cloning

CRISPRa

To activate the 3′RR IgH enhancer, we exploited the CRISPRa technology (*40*). The sgRNA (hs1.2 and hs4) sequence was obtained from previously published report (*61*). Briefly, oligonucleotides were annealed in the following reaction: 10 μM guide sequence oligo, 10 μM reverse complement oligo, and 50 mM NaCl in tris-EDTA buffer with the cycling parameters of 95°C for 2 min and then ramp down to 25°C at 5°C/min. The annealed oligos were cloned into the sgRNA vector (pLH-spsgRNA2, Addgene, 64114)

using a Golden Gate Assembly strategy including 100 ng of circular sgRNA vector plasmid, 0.2 μM annealed oligos, 20 U of Bbs I restriction enzyme, 750 U of T7 DNA ligase (Enzymatics, L6020L), and 1× T7 ligase buffer with the cycling parameters of 37°C for 5 min, followed by 60°C for 5 min. Insertion of sgRNA was validated by Sanger sequencing (Genetic Analyzer, 3130xl). The pcDNA-dCas9-p300^{C} was purchased from Addgene (no. 61357). Briefly, 500 ng of dCas9-p300^{C} expression vector and 500 ng of individual gRNA expression vectors were transfected in Med12^{KD} cells, and cells were incubated for 48 hours. After the incubation, the cells were CIT (+)–stimulated for another 48 hours before collecting the cells used for subsequent analysis.

CRISPRi

To knockdown the endogenous Integrator complex components (IntS11 and IntS13), sgRNA sequences (two sets for each) were designed from (http://crispor.tefor.net/). The obtained sgRNA oligonucleotide were annealed as described above and cloned in pSPgRNA purchased from Addgene (no. 47108) using the Bbs I cloning site. The vector dCas9-KRAB-MeCP2 was purchased from Addgene (no. 11082). Briefly, 500 ng of dCas9 expression vector and 500 ng of equimolar pooled sets of gRNAs were transfected, and cells were incubated for 24 hours. After the incubation, the cells were CIT (+) stimulated for another 24 hours before collecting the cells used for subsequent analysis.

b-Isox–mediated precipitation

b-Isox–mediated protein precipitation was performed as described previously (*79*). The b-Isox was purchased (Sigma-Aldrich, T51161), dissolved in DMSO, and added to the cell lysates at 100 or 250 μM final concentrations. The reaction solutions were incubated at 4°C for 1 hour and then centrifuged at 14,000 rpm for 15 min. The pellets were washed twice with the wash buffer and resuspended in 2× SDS sample loading buffer. After SDS-PAGE, protein was detected by Western blotting using indicated antibodies. The antibodies used in this study are listed in table S2.

Statistical analysis

Error bars represent SDs from either independent experiments or independent samples. All statistical analyses were performed using GraphPad Prism, and the information about statistical methods is specified in figure legends. The numbers of independent experiments or biological replicate samples and *P* values [not significant (n.s.), $^{*}P < 0.05$] are provided in individual figures. $P < 0.05$ was considered statistically significant.

Supplementary Materials

This PDF file includes:

Supplementary Text
Figs. S1 to S6
Table S1
References

Other Supplementary Material for this manuscript includes the following:

Table S2

View/request a protocol for this paper from *Bio-protocol*.

REFERENCES AND NOTES

1. T. Honjo, M. Muramatsu, S. Fagarasan, AID: How does it aid antibody diversity? *Immunity* **20**, 659–668 (2004).
2. M. Muramatsu, K. Kinoshita, S. Fagarasan, S. Yamada, Y. Shinkai, T. Honjo, Class switch recombination and hypermutation require activation-induced cytidine deaminase (AID), a potential RNA editing enzyme. *Cell* **102**, 553–563 (2000).
3. P. Revy, T. Muto, Y. Levy, F. Geissmann, A. Plebani, O. Sanal, N. Catalan, M. Forveille, R. Dufourcq-Labelouse, A. Gennery, I. Tezcan, F. Ersoy, H. Kayserili, A. G. Ugazio, N. Brousse, M. Muramatsu, L. D. Notarangelo, K. Kinoshita, T. Honjo, A. Fischer, A. Durandy, Activation-induced cytidine deaminase (AID) deficiency causes the autosomal recessive form of the Hyper-IgM syndrome (HIGM2). *Cell* **102**, 565–575 (2000).
4. J. Stavnezer, J. E. Guikema, C. E. Schrader, Mechanism and regulation of class switch recombination. *Annu. Rev. Immunol.* **26**, 261–292 (2008).
5. F. W. Alt, T. Honjo, A. Radbruch, M. Reth, *Molecular Biology of B Cells* (Elsevier, 2015).
6. R. Wuerffel, L. Wang, F. Grigera, J. Manis, E. Selsing, T. Perlot, F. W. Alt, M. Cogne, E. Pinaud, A. L. Kenter, S-S synapsis during class switch recombination is promoted by distantly located transcriptional elements and activation-induced deaminase. *Immunity* **27**, 711–722 (2007).
7. S. Sabouri, M. Kobayashi, N. A. Begum, J. Xu, K. Hirota, T. Honjo, C-terminal region of activation-induced cytidine deaminase (AID) is required for efficient class switch recombination and gene conversion. *Proc. Natl. Acad. Sci. U.S.A.* **111**, 2253–2258 (2014).
8. E. Pinaud, A. A. Khamlichi, C. Le Morvan, M. Drouet, V. Nalesso, M. Le Bert, M. Cogne, Localization of the 3′ IgH locus elements that effect long-distance regulation of class switch recombination. *Immunity* **15**, 187–199 (2001).
9. C. Vincent-Fabert, R. Fiancette, E. Pinaud, V. Truffinet, N. Cogne, M. Cogne, Y. Denizot, Genomic deletion of the whole IgH 3′ regulatory region (hs3a, hs1,2, hs3b, and hs4) dramatically affects class switch recombination and Ig secretion to all isotypes. *Blood* **116**, 1895–1898 (2010).
10. P. Rouaud, C. Vincent-Fabert, A. Saintamand, R. Fiancette, M. Marquet, I. Robert, B. Reina-San-Martin, E. Pinaud, M. Cogne, Y. Denizot, The IgH 3′ regulatory region controls somatic hypermutation in germinal center B cells. *J. Exp. Med.* **210**, 1501–1507 (2013).
11. P. Rouaud, C. Vincent-Fabert, R. Fiancette, M. Cogne, E. Pinaud, Y. Denizot, Enhancers located in heavy chain regulatory region (hs3a, hs1,2, hs3b, and hs4) are dispensable for diversity of VDJ recombination. *J. Biol. Chem.* **287**, 8356–8360 (2012).
12. A. Dauba, A. A. Khamlichi, Long-range control of class switch recombination by transcriptional regulatory elements. *Front. Immunol.* **12**, 738216 (2021).
13. A. Saintamand, P. Rouaud, F. Saad, G. Rios, M. Cogne, Y. Denizot, Elucidation of IgH 3′ region regulatory role during class switch recombination via germline deletion. *Nat. Commun.* **6**, 7084 (2015).
14. W. A. Dunnick, J. Shi, J. M. Zerbato, C. A. Fontaine, J. T. Collins, Enhancement of antibody class-switch recombination by the cumulative activity of four separate elements. *J. Immunol.* **187**, 4733–4743 (2011).
15. S. Schoenfelder, P. Fraser, Long-range enhancer-promoter contacts in gene expression control. *Nat. Rev. Genet.* **20**, 437–455 (2019).
16. A. Sanyal, B. R. Lajoie, G. Jain, J. Dekker, The long-range interaction landscape of gene promoters. *Nature* **489**, 109–113 (2012).
17. A. Panigrahi, B. W. O'Malley, Mechanisms of enhancer action: The known and the unknown. *Genome Biol.* **22**, 108 (2021).
18. S. W. Park, G. Li, Y. P. Lin, M. J. Barrero, K. Ge, R. G. Roeder, L. N. Wei, Thyroid hormone-induced juxtaposition of regulatory elements/factors and chromatin remodeling of Crabp1 dependent on MED1/TRAP220. *Mol. Cell* **19**, 643–653 (2005).
19. Q. Wang, J. S. Carroll, M. Brown, Spatial and temporal recruitment of androgen receptor and its coactivators involves chromosomal looping and polymerase tracking. *Mol. Cell* **19**, 631–642 (2005).
20. J. Soutourina, Transcription regulation by the Mediator complex. *Nat. Rev. Mol. Cell Biol.* **19**, 262–274 (2018).
21. B. L. Allen, D. J. Taatjes, The Mediator complex: A central integrator of transcription. *Nat. Rev. Mol. Cell Biol.* **16**, 155–166 (2015).
22. B. Aranda-Orgilles, R. Saldana-Meyer, E. Wang, E. Trompouki, A. Fassl, S. Lau, J. Mullenders, P. P. Rocha, R. Raviram, M. Guillamot, M. Sanchez-Diaz, K. Wang, C. Kayembe, N. Zhang, L. Amoasii, A. Choudhuri, J. A. Skok, M. Schober, D. Reinberg, P. Sicinski, H. Schrewe, A. Tsirigos, L. I. Zon, I. Aifantis, MED12 regulates HSC-specific enhancers independently of mediator kinase activity to control hematopoiesis. *Cell Stem Cell* **19**, 784–799 (2016).
23. M. T. Knuesel, K. D. Meyer, C. Bernecky, D. J. Taatjes, The human CDK8 subcomplex is a molecular switch that controls Mediator coactivator function. *Genes Dev.* **23**, 439–451 (2009).
24. C. B. Fant, D. J. Taatjes, Regulatory functions of the Mediator kinases CDK8 and CDK19. *Transcription* **10**, 76–90 (2019).

25. S. Srivastava, R. Kulshreshtha, Insights into the regulatory role and clinical relevance of mediator subunit, MED12, in human diseases. *J. Cell. Physiol.* **236**, 3163–3177 (2021).
26. D. Cheng, V. Vemulapalli, Y. Lu, J. Shen, S. Aoyagi, C. J. Fry, Y. Yang, C. E. Foulds, F. Stossi, L. S. Trevino, M. A. Mancini, B. W. O'Malley, C. L. Walker, T. G. Boyer, M. T. Bedford, CARM1 methylates MED12 to regulate its RNA-binding ability. *Life Sci Alliance* **1**, e201800117 (2018).
27. L. Wang, H. Zeng, Q. Wang, Z. Zhao, T. G. Boyer, X. Bian, W. Xu, MED12 methylation by CARM1 sensitizes human breast cancer cells to chemotherapy drugs. *Sci. Adv.* **1**, e1500463 (2015).
28. Z. Rubin, D. K. Grange, M. A. Cooper, Siblings with a novel MED12 variant and Odho syndrome with immune defects. *Clin. Genet.* **98**, 308–310 (2020).
29. M. Nakamura, S. Kondo, M. Sugai, M. Nazarea, S. Imamura, T. Honjo, High frequency class switching of an IgM+ B lymphoma clone CH12F3 to IgA+ cells. *Int. Immunol.* **8**, 193–201 (1996).
30. C. E. Schrader, E. K. Linehan, S. N. Mochegova, R. T. Woodland, J. Stavnezer, Inducible DNA breaks in Ig S regions are dependent on AID and UNG. *J. Exp. Med.* **202**, 561–568 (2005).
31. C. Boboila, V. Oksenych, M. Gostissa, J. H. Wang, S. Zha, Y. Zhang, H. Chai, C. S. Lee, M. Jankovic, L. M. Saez, M. C. Nussenzweig, P. J. McKinnon, F. W. Alt, B. Schwer, Robust chromosomal DNA repair via alternative end-joining in the absence of x-ray repair cross-complementing protein 1 (XRCC1). *Proc. Natl. Acad. Sci. U.S.A.* **109**, 2473–2478 (2012).
32. H. Ogiwara, A. Ui, A. Otsuka, H. Satoh, I. Yokomi, S. Nakajima, A. Yasui, J. Yokota, T. Kohno, Histone acetylation by CBP and p300 at double-strand break sites facilitates SWI/SNF chromatin remodeling and the recruitment of non-homologous end joining factors. *Oncogene* **30**, 2135–2146 (2011).
33. Q. Liu, S. Bischof, C. J. Harris, Z. Zhong, L. Zhan, C. Nguyen, A. Rashoff, W. D. Barshop, F. Sun, S. Feng, M. Potok, J. Gallego-Bartolome, J. Zhai, J. A. Wohlschlegel, M. F. Carey, J. A. Long, S. E. Jacobsen, The characterization of Mediator 12 and 13 as conditional positive gene regulators in *Arabidopsis*. *Nat. Commun.* **11**, 2798 (2020).
34. H. E. Pelish, B. B. Liau, I. I. Nitulescu, A. Tangpeerachaikul, Z. C. Poss, D. H. Da Silva, B. T. Caruso, A. Arefolov, O. Fadeyi, A. L. Christie, K. Du, D. Banka, E. V. Schneider, A. Jestel, G. Zou, C. Si, C. C. Ebmeier, R. T. Bronson, A. V. Krivtsov, A. G. Myers, N. E. Kohl, A. L. Kung, S. A. Armstrong, M. E. Lemieux, D. J. Taatjes, M. D. Shair, Mediator kinase inhibition further activates super-enhancer-associated genes in AML. *Nature* **526**, 273–276 (2015).
35. Z. C. Poss, C. C. Ebmeier, A. T. Odell, A. Tangpeerachaikul, T. Lee, H. E. Pelish, M. D. Shair, R. D. Dowell, W. M. Old, D. J. Taatjes, Identification of mediator kinase substrates in human cells using cortistatin A and quantitative phosphoproteomics. *Cell Rep.* **15**, 436–450 (2016).
36. M. Turunen, J. M. Spaeth, S. Keskitalo, M. J. Park, T. Kivioja, A. D. Clark, N. Makinen, F. Gao, K. Palin, H. Nurkkala, A. Vaharautio, M. Aavikko, K. Kampjarvi, P. Vahteristo, C. A. Kim, L. A. Aaltonen, M. Varjosalo, J. Taipale, T. G. Boyer, Uterine leiomyoma-linked MED12 mutations disrupt mediator-associated CDK activity. *Cell Rep.* **7**, 654–660 (2014).
37. N. A. Begum, A. Stanlie, M. Nakata, H. Akiyama, T. Honjo, The histone chaperone Spt6 is required for activation-induced cytidine deaminase target determination through H3K4me3 regulation. *J. Biol. Chem.* **287**, 32415–32429 (2012).
38. A. Stanlie, M. Aida, M. Muramatsu, T. Honjo, N. A. Begum, Histone3 lysine4 trimethylation regulated by the facilitates chromatin transcription complex is critical for DNA cleavage in class switch recombination. *Proc. Natl. Acad. Sci. U.S.A.* **107**, 22190–22195 (2010).
39. Z. Xu, Z. Fulop, G. Wu, E. J. Pone, J. Zhang, T. Mai, L. M. Thomas, A. Al-Qahtani, C. A. White, S. R. Park, P. Steinacker, Z. Li, J. Yates III, B. Herron, M. Otto, H. Zan, H. Fu, P. Casali, 14-3-3 adaptor proteins recruit AID to 5′-AGCT-3′-rich switch regions for class switch recombination. *Nat. Struct. Mol. Biol.* **17**, 1124–1135 (2010).
40. I. B. Hilton, A. M. D'Ippolito, C. M. Vockley, P. I. Thakore, G. E. Crawford, T. E. Reddy, C. A. Gersbach, Epigenome editing by a CRISPR-Cas9-based acetyltransferase activates genes from promoters and enhancers. *Nat. Biotechnol.* **33**, 510–517 (2015).
41. A. Visel, E. M. Rubin, L. A. Pennacchio, Genomic views of distant-acting enhancers. *Nature* **461**, 199–205 (2009).
42. W. A. Dunnick, J. Shi, C. Fontaine, J. T. Collins, Transgenes of the mouse immunoglobulin heavy chain locus, lacking distal elements in the 3′ regulatory region, are impaired for class switch recombination. *PLOS ONE* **8**, e55842 (2013).
43. J. Laurencikiene, V. Deveikaite, E. Severinson, HS1,2 enhancer regulation of germline epsilon and gamma2b promoters in murine B lymphocytes: Evidence for specific promoter-enhancer interactions. *J. Immunol.* **167**, 3257–3265 (2001).
44. C. Chauveau, M. Cogne, Palindromic structure of the IgH 3′locus control region. *Nat. Genet.* **14**, 15–16 (1996).
45. S. Peron, B. Laffleur, N. Denis-Lagache, J. Cook-Moreau, A. Tinguely, L. Delpy, Y. Denizot, E. Pinaud, M. Cogne, AID-driven deletion causes immunoglobulin heavy chain locus suicide recombination in B cells. *Science* **336**, 931–934 (2012).
46. N. Hah, C. G. Danko, L. Core, J. J. Waterfall, A. Siepel, J. T. Lis, W. L. Kraus, A rapid, extensive, and transient transcriptional response to estrogen signaling in breast cancer cells. *Cell* **145**, 622–634 (2011).
47. W. W. Gao, R. Q. Xiao, W. J. Zhang, Y. R. Hu, B. L. Peng, W. J. Li, Y. H. He, H. F. Shen, J. C. Ding, Q. X. Huang, T. Y. Ye, Y. Li, Z. Y. Liu, R. Ding, M. G. Rosenfeld, W. Liu, JMJD6 licenses ERα-dependent enhancer and coding gene activation by modulating the recruitment of the CARM1/MED12 co-activator complex. *Mol. Cell* **70**, 340–357.e8 (2018).
48. D. A. Bose, G. Donahue, D. Reinberg, R. Shiekhattar, R. Bonasio, S. L. Berger, RNA binding to CBP stimulates histone acetylation and transcription. *Cell* **168**, 135–149.e22 (2017).
49. F. Lai, U. A. Orom, M. Cesaroni, M. Beringer, D. J. Taatjes, G. A. Blobel, R. Shiekhattar, Activating RNAs associate with Mediator to enhance chromatin architecture and transcription. *Nature* **494**, 497–501 (2013).
50. S. J. Nair, L. Yang, D. Meluzzi, S. Oh, F. Yang, M. J. Friedman, S. Wang, T. Suter, I. Alshareedah, A. Gamliel, Q. Ma, J. Zhang, Y. Hu, Y. Tan, K. A. Ohgi, R. S. Jayani, P. R. Banerjee, A. K. Aggarwal, M. G. Rosenfeld, Phase separation of ligand-activated enhancers licenses cooperative chromosomal enhancer assembly. *Nat. Struct. Mol. Biol.* **26**, 193–203 (2019).
51. B. R. Sabari, A. Dall'Agnese, A. Boija, I. A. Klein, E. L. Coffey, K. Shrinivas, B. J. Abraham, N. M. Hannett, A. V. Zamudio, J. C. Manteiga, C. H. Li, Y. E. Guo, D. S. Day, J. Schuijers, E. Vasile, S. Malik, D. Hnisz, T. I. Lee, I. I. Cisse, R. G. Roeder, P. A. Sharp, A. K. Chakraborty, R. A. Young, Coactivator condensation at super-enhancers links phase separation and gene control. *Science* **361**, eaar3958 (2018).
52. J. Dong, R. A. Panchakshari, T. Zhang, Y. Zhang, J. Hu, S. A. Volpi, R. M. Meyers, Y. J. Ho, Z. Du, D. F. Robbiani, F. Meng, M. Gostissa, M. C. Nussenzweig, J. P. Manis, F. W. Alt, Orientation-specific joining of AID-initiated DNA breaks promotes antibody class switching. *Nature* **525**, 134–139 (2015).
53. K. Yu, M. R. Lieber, Current insights into the mechanism of mammalian immunoglobulin class switch recombination. *Crit. Rev. Biochem. Mol. Biol.* **54**, 333–351 (2019).
54. A. Stanlie, A. S. Yousif, H. Akiyama, T. Honjo, N. A. Begum, Chromatin reader Brd4 functions in Ig class switching as a repair complex adaptor of nonhomologous end-joining. *Mol. Cell* **55**, 97–110 (2014).
55. N. A. Begum, F. Haque, A. Stanlie, A. Husain, S. Mondal, M. Nakata, T. Taniguchi, H. Taniguchi, T. Honjo, Phf5a regulates DNA repair in class switch recombination via p400 and histone H2A variant deposition. *EMBO J.* **40**, e106393 (2021).
56. A. S. Thomas-Claudepierre, I. Robert, P. P. Rocha, R. Raviram, E. Schiavo, V. Heyer, R. Bonneau, V. M. Luo, J. K. Reddy, T. Borggrefe, J. A. Skok, B. Reina-San-Martin, Mediator facilitates transcriptional activation and dynamic long-range contacts at the IgH locus during class switch recombination. *J. Exp. Med.* **213**, 303–312 (2016).
57. E. Calo, J. Wysocka, Modification of enhancer chromatin: What, how, and why? *Mol. Cell* **49**, 825–837 (2013).
58. W. Li, D. Notani, M. G. Rosenfeld, Enhancers as non-coding RNA transcription units: Recent insights and future perspectives. *Nat. Rev. Genet.* **17**, 207–223 (2016).
59. F. Lai, A. Gardini, A. Zhang, R. Shiekhattar, Integrator mediates the biogenesis of enhancer RNAs. *Nature* **525**, 399–403 (2015).
60. V. Delgado-Benito, D. B. Rosen, Q. Wang, A. Gazumyan, J. A. Pai, T. Y. Oliveira, D. Sundaravinayagam, W. Zhang, M. Andreani, L. Keller, K. R. Kieffer-Kwon, A. Pekowska, S. Jung, M. Driesner, R. I. Subbotin, R. Casellas, B. T. Chait, M. C. Nussenzweig, M. Di Virgilio, The chromatin reader ZMYND8 regulates Igh enhancers to promote immunoglobulin class switch recombination. *Mol. Cell* **72**, 636–649.e8 (2018).
61. J. Fitz, T. Neumann, M. Steininger, E. M. Wiedemann, A. C. Garcia, A. Athanasiadis, U. E. Schoeberl, R. Pavri, Spt5-mediated enhancer transcription directly couples enhancer activation with physical promoter interaction. *Nat. Genet.* **52**, 505–515 (2020).
62. R. Pavri, A. Gazumyan, M. Jankovic, M. Di Virgilio, I. Klein, C. Ansarah-Sobrinho, W. Resch, A. Yamane, B. Reina San-Martin, V. Barreto, T. J. Nieland, D. E. Root, R. Casellas, M. C. Nussenzweig, Activation-induced cytidine deaminase targets DNA at sites of RNA polymerase II stalling by interaction with Spt5. *Cell* **143**, 122–133 (2010).
63. L. M. Soares, P. C. He, Y. Chun, H. Suh, T. Kim, S. Buratowski, Determinants of histone H3K4 methylation patterns. *Mol. Cell* **68**, 773–785.e6 (2017).
64. B. Vaidyanathan, J. Chaudhuri, Epigenetic codes programing class switch recombination. *Front. Immunol.* **6**, 405 (2015).
65. L. Wang, R. Wuerffel, S. Feldman, A. A. Khamlichi, A. L. Kenter, S region sequence, RNA polymerase II, and histone modifications create chromatin accessibility during class switch recombination. *J. Exp. Med.* **206**, 1817–1830 (2009).
66. H. Zan, P. Casali, Epigenetics of peripheral B-cell differentiation and the antibody response. *Front. Immunol.* **6**, 631 (2015).
67. J. A. Daniel, M. A. Santos, Z. Wang, C. Zang, K. R. Schwab, M. Jankovic, D. Filsuf, H. T. Chen, A. Gazumyan, A. Yamane, Y. W. Cho, H. W. Sun, K. Ge, W. Peng, M. C. Nussenzweig, R. Casellas, G. R. Dressler, K. Zhao, A. Nussenzweig, PTIP promotes chromatin changes critical for immunoglobulin class switch recombination. *Science* **329**, 917–923 (2010).
68. G. Li, C. A. White, T. Lam, E. J. Pone, D. C. Tran, K. L. Hayama, H. Zan, Z. Xu, P. Casali, Combinatorial H3K9acS10ph histone modification in IgH locus S regions targets 14-3-3 adaptors and AID to specify antibody class-switch DNA recombination. *Cell Rep.* **5**, 702–714 (2013).

69. W. Li, D. Notani, Q. Ma, B. Tanasa, E. Nunez, A. Y. Chen, D. Merkurjev, J. Zhang, K. Ohgi, X. Song, S. Oh, H. S. Kim, C. K. Glass, M. G. Rosenfeld, Functional roles of enhancer RNAs for oestrogen-dependent transcriptional activation. *Nature* **498**, 516–520 (2013).
70. A. A. Sigova, B. J. Abraham, X. Ji, B. Molinie, N. M. Hannett, Y. E. Guo, M. Jangi, C. C. Giallourakis, P. A. Sharp, R. A. Young, Transcription factor trapping by RNA in gene regulatory elements. *Science* **350**, 978–981 (2015).
71. M. Kato, T. W. Han, S. Xie, K. Shi, X. Du, L. C. Wu, H. Mirzaei, E. J. Goldsmith, J. Longgood, J. Pei, N. V. Grishin, D. E. Frantz, J. W. Schneider, S. Chen, L. Li, M. R. Sawaya, D. Eisenberg, R. Tycko, S. L. McKnight, Cell-free formation of RNA granules: Low complexity sequence domains form dynamic fibers within hydrogels. *Cell* **149**, 753–767 (2012).
72. P. Prontera, V. Ottaviani, D. Rogaia, I. Isidori, A. Mencarelli, N. Malerba, D. Cocciadiferro, P. Rolph, G. Stangoni, A. Vulto-van Silfhout, G. Merla, A novel MED12 mutation: Evidence for a fourth phenotype. *Am. J. Med. Genet. A* **170**, 2377–2382 (2016).
73. T. E. Prescott, M. A. Kulseth, K. R. Heimdal, B. Stadheim, E. Hopp, T. Gambin, Z. H. Coban Akdemir, S. N. Jhangiani, D. M. Muzny, R. A. Gibbs, J. R. Lupski, A. Stray-Pedersen, Two male sibs with severe micrognathia and a missense variant in MED12. *Eur. J. Med. Genet.* **59**, 367–372 (2016).
74. M. Behrends, O. Engmann, Loop interrupted: Dysfunctional chromatin relations in neurological diseases. *Front. Genet.* **12**, 732033 (2021).
75. S. Heinz, C. E. Romanoski, C. Benner, C. K. Glass, The selection and function of cell type-specific enhancers. *Nat. Rev. Mol. Cell Biol.* **16**, 144–154 (2015).
76. R. Nativio, Y. Lan, G. Donahue, S. Sidoli, A. Berson, A. R. Srinivasan, O. Shcherbakova, A. Amlie-Wolf, J. Nie, X. Cui, C. He, L. S. Wang, B. A. Garcia, J. Q. Trojanowski, N. M. Bonini, S. L. Berger, An integrated multi-omics approach identifies epigenetic alterations associated with Alzheimer's disease. *Nat. Genet.* **52**, 1024–1035 (2020).
77. R. Madabhushi, L. Pan, L. H. Tsai, DNA damage and its links to neurodegeneration. *Neuron* **83**, 266–282 (2014).
78. W. Wu, S. E. Hill, W. J. Nathan, J. Paiano, E. Callen, D. Wang, K. Shinoda, N. van Wietmarschen, J. M. Colon-Mercado, D. Zong, R. De Pace, H. Y. Shih, S. Coon, M. Parsadanian, R. Pavani, H. Hanzlikova, S. Park, S. K. Jung, P. J. McHugh, A. Canela, C. Chen, R. Casellas, K. W. Caldecott, M. E. Ward, A. Nussenzweig, Neuronal enhancers are hotspots for DNA single-strand break repair. *Nature* **593**, 440–444 (2021).
79. M. D. Panas, N. Kedersha, G. M. McInerney, Methods for the characterization of stress granules in virus infected cells. *Methods* **90**, 57–64 (2015).
80. H. Murakami, Y. Enomoto, Y. Tsurusaki, Y. Sugio, K. Kurosawa, A female patient with X-linked Ohdo syndrome of the Maat-Kievit-Brunner phenotype caused by a novel variant of MED12. *Congenit. Anom.* **60**, 91–93 (2020).
81. N. Fieremans, H. Van Esch, M. Holvoet, G. Van Goethem, K. Devriendt, M. Rosello, S. Mayo, F. Martinez, S. Jhangiani, D. M. Muzny, R. A. Gibbs, J. R. Lupski, J. R. Vermeesch, P. Marynen, G. Froyen, Identification of intellectual disability genes in female patients with a skewed X-inactivation pattern. *Hum. Mutat.* **37**, 804–811 (2016).
82. J. Zhang, J. Baran, A. Cros, J. M. Guberman, S. Haider, J. Hsu, Y. Liang, E. Rivkin, J. Wang, B. Whitty, M. Wong-Erasmus, L. Yao, A. Kasprzyk, International Cancer Genome Consortium Data Portal—A one-stop shop for cancer genomics data. *Database* **2011**, bar026 (2011).
83. L. M. Donnio, B. Bidon, S. Hashimoto, M. May, A. Epanchintsev, C. Ryan, W. Allen, A. Hackett, J. Gecz, C. Skinner, R. E. Stevenson, A. P. M. de Brouwer, C. Coutton, C. Francannet, P. S. Jouk, C. E. Schwartz, J. M. Egly, MED12-related XLID disorders are dose-dependent of immediate early genes (IEGs) expression. *Hum. Mol. Genet.* **26**, 2062–2075 (2017).
84. P. Rump, R. C. Niessen, K. T. Verbruggen, O. F. Brouwer, M. de Raad, R. Hordijk, A novel mutation in MED12 causes FG syndrome (Opitz-Kaveggia syndrome). *Clin. Genet.* **79**, 183–188 (2011).
85. H. Risheg, J. M. Graham Jr., R. D. Clark, R. C. Rogers, J. M. Opitz, J. B. Moeschler, A. P. Peiffer, M. May, S. M. Joseph, J. R. Jones, R. E. Stevenson, C. E. Schwartz, M. J. Friez, A recurrent mutation in MED12 leading to R961W causes Opitz-Kaveggia syndrome. *Nat. Genet.* **39**, 451–453 (2007).
86. C. E. Schwartz, P. S. Tarpey, H. A. Lubs, A. Verloes, M. M. May, H. Risheg, M. J. Friez, P. A. Futreal, S. Edkins, J. Teague, S. Briault, C. Skinner, A. Bauer-Carlin, R. J. Simensen, S. M. Joseph, J. R. Jones, J. Gecz, M. R. Stratton, F. L. Raymond, R. E. Stevenson, The original Lujan syndrome family has a novel missense mutation (p.N1007S) in the MED12 gene. *J. Med. Genet.* **44**, 472–477 (2007).
87. B. Isidor, T. Lefebvre, C. Le Vaillant, G. Caillaud, L. Faivre, F. Jossic, M. Joubert, N. Winer, C. Le Caignec, G. Borck, A. Pelet, J. Amiel, A. Toutain, N. Ronce, M. Raynaud, A. Verloes, A. David, Blepharophimosis, short humeri, developmental delay and hirschsprung disease: Expanding the phenotypic spectrum of MED12 mutations. *Am. J. Med. Genet. A* **164A**, 1821–1825 (2014).
88. K. Kampjarvi, N. H. Kim, S. Keskitalo, A. D. Clark, P. von Nandelstadh, M. Turunen, T. Heikkinen, M. J. Park, N. Makinen, K. Kivinummi, S. Lintula, K. Hotakainen, H. Nevanlinna, P. Hokland, T. Bohling, R. Butzow, J. Bohm, J. P. Mecklin, H. Jarvinen, M. Kontro, T. Visakorpi, J. Taipale, M. Varjosalo, T. G. Boyer, P. Vahteristo, Somatic MED12 mutations in prostate cancer and uterine leiomyomas promote tumorigenesis through distinct mechanisms. *Prostate* **76**, 22–31 (2016).
89. K. G. Langley, J. Brown, R. J. Gerber, J. Fox, M. J. Friez, M. Lyons, S. A. Schrier Vergano, Beyond Ohdo syndrome: A familial missense mutation broadens the MED12 spectrum. *Am. J. Med. Genet. A* **167A**, 3180–3185 (2015).

Acknowledgments: We thank M. D. Shair and D. J. Taatjes for providing the Med12 kinase inhibitor (CA). F.H. also thanks his wife Samina for moral support and his mentor T. Honjo for arranging and providing the postdoctoral fellowship. We also thank M. Nakata for technical assistance. **Funding:** This work was supported by funding from the Japan Society for the Promotion of Science; Grants-in-Aid for Scientific Research (S) 22H00449 to T.H. and Grants-in-Aid for Scientific Research (C) 21K06015 to N.A.B. **Author contributions:** F.H., N.A.B., and T.H. conceptualized, designed, and wrote the manuscript. F.H. performed the experiments. T.H. and N.A.B. supervised the project. F.H., N.A.B., and T.H. reviewed the manuscript. **Competing interests:** The authors declare that they have no competing interests. **Data and materials availability:** All data needed to evaluate the conclusions in the paper are present in the paper and/or the Supplementary Materials. This study includes no data deposited in external repositories.

Submitted 24 May 2022
Accepted 27 October 2022
Published 25 November 2022
10.1126/sciadv.add1466